Ribbed bedforms in palaeo-ice streams reveal shear margin positions, lobe shutdown and the interaction of meltwater drainage and ice velocity patterns

Jean Vérité[1], Édouard Ravier[1], Olivier Bourgeois[2], Stéphane Pochat[2], Thomas Lelandais[1], Régis Mourgues[1], Christopher D. Clark[3], Paul Bessin[1], David Peigné[1], Nigel Atkinson[4]

[1] Laboratoire de Planétologie et Géodynamique, UMR 6112, CNRS, Le Mans Université, Avenue Olivier Messiaen, 72085 Le Mans CEDEX 9, France
[2] Laboratoire de Planétologie et Géodynamique, UMR 6112, CNRS, Université de Nantes, 2 rue de la Houssinière, BP 92208, 44322 Nantes CEDEX 3, France
[3] Department of Geography, University of Sheffield, Sheffield, UK
[4] Alberta Geological Survey, 4th Floor Twin Atria Building, 4999-98 Ave. Edmonton, AB, T6B 2X3, Canada

Correspondence to: Jean Vérité (jean.verite@univ-lemans.fr)

Abstract.

Conceptual ice stream landsystems derived from geomorphological and sedimentological observations provide constraints on ice-meltwater-till-bedrock interactions on palaeo-ice stream beds. Within these landsystems, the spatial distribution and formation processes of ribbed bedforms remain unclear. We explore the conditions under which these bedforms develop and their spatial organisation with (i) an experimental model that reproduces the dynamics of ice streams and subglacial landsystems and (ii) an analysis of the distribution of ribbed bedforms on selected examples of paleo-ice stream beds of the Laurentide Ice Sheet. We find that a specific kind of ribbed bedforms can develop subglacially from a flat bed beneath shear margins (i.e., lateral ribbed bedforms) and lobes (i.e., submarginal ribbed bedforms) of ice streams. These bedforms initiate where the ice flow undergoes high velocity gradients and the ice-bed interface is unlubricated. We suggest that (i) their orientation reflects the local stress state along the ice-bed interface and (ii) their development reveals distinctive types of subglacial drainage patterns below these two kinds of margins: linked-cavities and efficient meltwater channels respectively. These ribbed bedforms are thus convenient geomorphic markers to reconstruct palaeo-ice stream margins and constrain palaeo-ice flow dynamics and palaeo-meltwater drainage characteristics.

1. Introduction

The dynamics of ice sheets is largely controlled by the activity of narrow corridors of fast-flowing ice, named ice streams (Paterson, 1994). In Antarctica, 10% of the ice sheet is covered by ice streams and 90% of the ice sheet is estimated to discharge through these corridors that flow at a few hundreds of m·y^{-1} (Bamber et al., 2000). Studies on modern ice streams – through satellite imagery, boreholes and geophysics – have improved our understanding of the influence of ice streams on the mass balance of ice sheets. Many investigations highlight the role of shear margins on the overall stress balance of ice streams and the importance of imparted drag here, along with basal drag in controlling flow speed and ice stream width (Engelhardt et al., 1990; Goldstein et al., 1993; Echelmeyer et al., 1994; Tulaczyk et al., 2000; Raymond et al., 2001). A lack of knowledge remains however on the spatial and temporal evolution of basal conditions beneath ice streams (e.g., distribution of basal shear stresses, meltwater drainage patterns) and on the processes acting at the ice-bed interface during the formation of subglacial bedforms. This is because basal investigations on modern ice streams are restricted to

1

punctual observations. Palaeoglaciology aims to fill this gap by using the geomorphological and sedimentological record of former ice stream beds. Based on this approach, conceptual models of ice stream landsystems characterized by either

40 synchronous or time-transgressive imprints have been developed (Dyke and Morris, 1988; Kleman and Borgström, 1996; Clark and Stokes, 2003).

Even though a general model of ice stream landsystems is now well-established, the genesis of some landforms in these landsystems remains debated, notably regarding their relation to ice dynamics and subglacial meltwater drainage. After mega-scale glacial lineations and drumlins, ribbed bedforms potentially represent some of the most conspicuous and

45 ubiquitous landforms on palaeo-ice stream beds, although to date, their distribution is not clearly accommodated in ice stream landsystem models (Dyke et al., 1992; Clark and Stokes 2001; Stokes et al., 2007), and their formation is explained by a variety of interpretations (Boulton, 1987; Hättestrand and Kleman, 1999; Lindén et al., 2008; Fowler and Chapwanya, 2014), which typically focus on variations in basal shear stress, ice velocity and ice-bed coupling-decoupling resulting from local transitions in basal conditions (e.g. lubricated-unlubricated and/or cold-warm). Such velocity gradients and

50 changes in basal conditions are observed across the shear margins (Raymond et al., 2001) and lobe margins (for terrestrial-terminating ice streams; Patterson, 1997) of ice streams. These margins should therefore constitute preferential areas for the formation of ribbed bedforms. However, a possible relation between ribbed bedforms and ice stream margins has so far not been reported.

Here, we re-examine the formation and distribution of ribbed bedforms in the ice stream landsystem. We provide new

55 constraints regarding their formation and distribution beneath ice stream margins by comparing results from experimental modelling and palaeo-glaciological investigations. For that purpose, we developed an experimental model that reproduces ice stream dynamics together with the evolution of subglacial bedforms and meltwater drainage. From remotely-sensed images and topographic data, we also mapped ribbed bedforms below shear and lobe margins of palaeo-ice streams of the Laurentide Ice Sheet. By combining the experimental and geomorphological approaches, we propose an integrated

60 morpho-hydro-glaciological model for the formation of ribbed bedforms associated with ice stream margins. We finally integrate ribbed bedforms into the ice stream landsystem and discuss their palaeo-glaciological implications for the mapping of palaeo-ice streams and the reconstruction of past subglacial hydrology and ice stream dynamics.
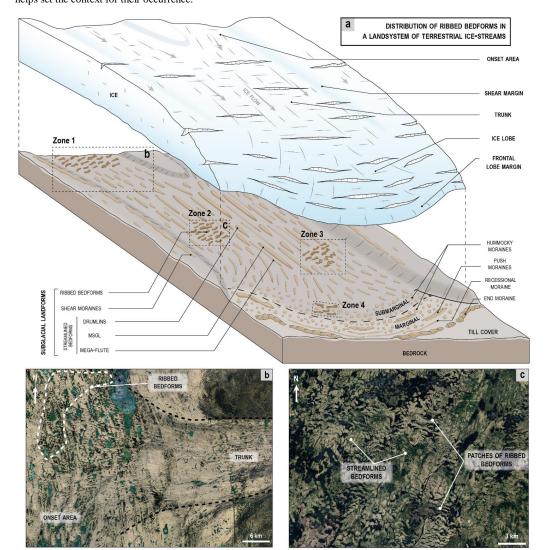
2. Ribbed bedforms in ice stream landsystems

2.1. The general model of an ice stream landsystem

65 Glaciological, geomorphological and sedimentological studies on terrestrial- and marine-terminating ice streams have enabled the development of a general landsystem model (**Fig. 1a**; Dyke and Morris, 1988; Kleman and Borgström, 1996; Clark and Stokes, 2003), which is critical for reconstructing spatial and temporal variations in the distribution of palaeo-ice streams, as well as understanding the process-form relationships of their geomorphic imprints across the landscape (Denton and Hughes, 1981; Patterson, 1997; Winsborrow et al., 2004; Margold et al., 2015). The areas where the ice

70 starts channelizing in the upstream part of ice streams (i.e. onset areas) are characterized by slow ice flow and a large spectrum of flow orientations due to the convergence of multiple tributaries. Ice is then incorporated within narrow and well-defined trunks delimited by abrupt lateral shear margins, feeding channels with high flow velocities (>300 $m\cdot y^{-1}$; Clark and Stokes, 2003). Terminal zones of ice streams are characterized either by marine-based ice shelves and calving fronts, or land-based marginal lobation (Stokes and Clark, 2001).

75 Here we summarise landform generation, their relation with the local ice dynamics and their distribution within ice stream landsystem (i.e. onset areas, trunk, lateral and lobe margins), drawn from observations and interpretations made in the

palaeo ice stream literature. A special concern is given to ribbed bedforms and their different modes of formation, which helps set the context for their occurrence.

Figure 1. (a) Distribution of ribbed bedforms, as currently envisaged, in an "ideal" isochronous landsystem of terrestrial palaeo-ice stream (modified after Clark and Stokes, 2003). (b) Ribbed bedforms located in the cold-based onset area (Zone 1), upstream of the streamlined bedforms recording the warm-based trunk of an ice stream (Fisher Lake, Prince of Wales Island, Canada). (c) Patches of ribbed bedforms with abrupt borders with surrounding streamlined bedforms (Zone 2; Lake Naococane, Canada). Also documented, and shown on a), but not shown with specific examples are progressive downstream transitions from ribbed bedforms to drumlins (Zone 3) and marginal relationships between hummocky and ribbed bedforms (Zone 4) (© Landsat / Copernicus - © Google Earth).

2.1.1. Streamlined bedforms: markers of fast ice flow in ice stream trunks

Trunks constitute corridors of overall fast ice flow that present transverse velocity gradients from their axes towards their shear margins (Sergienko and Hindmarsh, 2013; Zheng et al., 2019); longitudinal velocity gradients also occur for land-based ice streams (Patterson, 1997). The main glaciological criterion to identify palaeo-ice stream trunks is the presence of swarms of streamlined bedforms, such as mega-scale glacial lineations (MSGLs) and drumlins, elongated parallel to

ice flow direction (**Fig. 1**; Stokes and Clark, 2001; Clark and Stokes, 2003). These bedforms, mainly composed of subglacial soft sediments, can be up to hundreds of metres in width, tens to a hundred kilometres in length and metres in height (e.g. Menzies, 1979; Stokes and Clark, 2001). Sets of parallel mega-grooves (furrows within the substratum),

95 carved by boulders trapped and transported at the ice base, are sometimes described in paleo-ice stream trunks. They are typically 1 km in length, a few tens of metres in depth and frequently show a mega-raft at their downstream terminations and bordering ridges (Atkinson et al., 2016; Newton et al., 2018; Evans et al., 2020). Streamlined bedforms and grooves provide a relevant proxy for reconstructing ice flow velocity and direction (Dyke and Morris, 1988; Boyce and Eyles, 1991; Stokes and Clark, 2002a; Briner, 2007).

100 **2.1.2. Marginal and submarginal landforms: indicators of fluctuating ice lobes**

Terrestrially-terminating ice streams necessarily require broad ice lobes downstream of their trunks in order to have a sufficiently large ablation surface to lose mass, balancing (or not) ice delivered down the fast flowing trunk. It seems that imbalances are common leading to ice stream lobes typically being characterized by the alternation of surge, stagnation and retreat phases, and which control the types of landforms that develop at the margin (Evans et al., 1999, 2008). Surge

105 phases are marked by distributed meltwater discharge, which when it switches to channelized drainage reduces the widespread lubrication of the ice-bed interface, thus stabilizing the lobe through stagnation of its front (Patterson, 1997; Lelandais et al., 2018). Ice lobe retreat tends to follow the peak-phase of ice sheet collapse, characterized by the maximum advance of the lobe (e.g. Margold et al., 2018). Ice marginal/proglacial landforms result from processes of erosion, transport, deformation and deposition during these fluctuations and they form widespread belts of sediment ridges parallel

110 to palaeo-lobe margins (**Fig. 1a**). Push moraines are glaciotectonic asymmetrical ridges that result from bulldozing and thrusting of marginal sediments by surging lobes (Boulton, 1986; Benn and Evans, 2010). During perennial lobe stagnation or overall marginal retreat, processes of bulldozing are limited but sediments entrained within the ice are deposited by ablation into small ridges, called recessional moraines. In response to lobe re-advances, previously deposited marginal landforms can be pushed into composite ridges, producing large end moraines (Evans and Hiemstra, 2005;

115 Chandler et al., 2016), or submarginally remoulded by the overriding ice lobe, producing overridden moraines (Totten, 1969). However, no previous studies have described the subglacial formation of belts composed of transverse ridges mirroring the shape of lobate margins. Crevasse squeezed ridges (CSRs; non-reported on **Fig. 1** because of their potential widespread coverage), which are believed to form by the squeezing or injection of basal till into subglacial crevasses (Sharp, 1985), are landforms generally associated to the marginal to submarginal activity of ice lobes. Wide arcuate zones

120 of CSRs are related to widespread fracturing within glacier surge lobes, possibly in the context of surging ice streams, while narrow concentric arcs of CSRs, often associated to recessional push moraines, are related to submarginal till deformation at non-surging active glacier lobes (Evans et al., 2015; 2016).

Hummocky moraines are comprised of undulating and irregular circular mounds with no particular orientation, up to tens of metres in height and up to hundreds of metres in width, that generally occupy broad belts within ice-marginal and

125 submarginal landsystems (**Fig. 1a**; Benn, 1992; Johnson and Clayton, 2003). Formation models of hummocky moraines encompass (i) subglacial reshaping and squeezing of pre-existing till ridges inside stagnant ice cavities (Eyles et al., 1999; Boone and Eyles, 2001), (ii) deposition of (supra)glacial sediments by block melting in 'dead-ice' during deglaciation (Ebert and Kleman, 2004), (iii) infilling of sinkholes and moulins by supraglacial sediments (Johnson and Clayton, 2003) and (iv) local supraglacial concentrations of debris whose shapes are preserved after ice-sheet retreat (Kjær and Krüger,

130 2001). Thus, "hummocky" is a geomorphic term that may refer to various marginal landforms – till-cored moraines, rim ridges, circular morainic features, ice-cored/dead-ice moraines and 'doughnut' moraines – independently of their formation process.

2.1.3. Shear moraines: signature of velocity gradients in ice stream lateral margins

At the transition between the fast-flowing ice stream trunk and the surrounding slow-flowing ice sheet, lateral drag

135　accommodates the fraction of the driving stress that is not counterbalanced by the basal drag. The shear stress here results from a sharp gradient of ice velocity defining the lateral shear margins of ice streams (Echelmeyer et al., 1994; Raymond et al., 2001). Such shear margins have been described as zones with intense shear-heating, prolific crevassing and well-developed water drainage systems, which respectively promote the production, infiltration and convergence of meltwater at this boundary. The meltwater here is thought to encourage strong erosion of the substratum, and transport and

140　deposition of sediments responsible for the development of ice stream shear moraines (Dyke and Morris, 1988; Dyke et al., 1992; Stokes and Clark, 2002b). Shear moraines are typically continuous, linear and narrow ridges of till, tens of kilometres in length, less than 1 km in width and tens of metres in height (**Fig. 1a**). They are often used to map the boundaries of ice stream trunks often coinciding in position with the abrupt edge of streamlined bedforms such as MSGLs (e.g. Clark and Stokes 2001), and can safely be interpreted as recording the shear margin position of palaeo-ice streams.

145　CSR corridors have also been suggested to form along lateral shear zones between individual flow units within ice streams (Evans et al., 2016). Flow reorganisation triggered by the narrowing of the fast-flowing trunk prior to the shutdown of ice streams is proposed to explain the development of lateral shear and subsequent crevassing.

2.2. Distribution and formation of ribbed bedforms beneath ice streams

Ribbed bedforms are undulating ridges with a regular spacing, transverse to the palaeo-ice flow (**Fig. 1**). We use the term

150　"ribbed bedform" as a descriptive morphologic term, without a genetic connotation, and that merges a variety of apparently similar bedforms that have been labelled differently according to their size or geographic origin. This term embraces the following forms described in the literature: (i) Rogen moraines, short-scale ribbed bedforms firstly described on Rogen Lake in Sweden (Lundqvist, 1969), (ii) ribbed moraines, their North-American counterparts (Hughes, 1964), (iii) traction ribs, intermediate-scale ribbed bedforms (Sergienko and Hindmarsh, 2013; Stokes et al., 2016) and (iv) mega-

155　scale transverse bedforms (Greenwood and Kleman, 2010). Ribbed and Rogen moraines are hundreds of metres to a few kilometres in length, a few hundreds of metres in width and tens of metres in height (l/w = 2.5; Dunlop and Clark, 2006b). Mega-scale transverse bedforms are 20 to 40 km in length, 3 to 6 km in width (l/w = 5.7) and 5 to 10 m in height (Greenwood and Kleman, 2010). Both are depicted with an orthogonal to sub-orthogonal orientation relative to the local ice flow. Traction ribs are 1 to 6 km long, 0.4 to 1 km wide (l/w = 2.9) and 10 to 20 m high ; they are believed to form

160　perpendicular (90°) to oblique (20°) to ice flow direction (Sergienko and Hindmarsh, 2013; Stokes et al., 2016).
Ribbed bedforms are observed (i) outside of ice stream in the inner, cold-based, regions of ice sheets (Aylsworth and Shilts, 1989; Dyke et al., 1992; Hättestrand and Kleman, 1999; Stokes, 2018), (ii) in onset areas of ice streams at the transition between cold- and warm-based ice (**Fig. 1b - Zone 1**; Bouchard, 1989; Dyke et al., 1992; Hättestrand and Kleman, 1999), (iii) in ice stream trunks as isolated patches associated with streamlined bedforms (**Fig. 1c - Zones 2, 3**;

165　Cowan, 1968; Boulton and Hindmarsh, 1987; Aylsworth and Shilts, 1989; Bouchard, 1989; Dyke et al., 1992; Stokes and Clark, 2003, Stokes et al., 2006a, 2008) and (iv) in submarginal areas associated with hummocky moraines within stagnant ablation complexes (**Fig. 1 - Zone 4**; Marich et al., 2005; Möller, 2006, 2010).
Beneath warm-based ice streams, ribbed bedforms frequently form at localized areas of ice flow slowdown (i.e. sticky-spots, Stokes et al., 2007, 2016) due to transitions and variations in the basal thermal regime and/or in the basal shear

170　stress. Four major formation processes are proposed for ribbed bedforms: (i) overriding, deformation or reshaping of pre-existing sedimentary mounds, such as former streamlined or marginal landforms (Boulton, 1987; Lundqvist, 1989; Möller, 2006), (ii) ice-fracturing along transitions of warm-to-cold ice base, where tensional stresses increase (Hättestrand

and Kleman, 1999; Sarala, 2006), (iii) folding and thrusting of subglacial sediment or sediment-rich basal ice in response to bed heterogeneities, such as cold ice-base, dewatered till and topographic relief (Shaw, 1979; Bouchard, 1989; Lindén

175   et al., 2008; Stokes et al., 2008) and (iv) in-situ generation of naturally arising instabilities in the coupled flow of ice, water and sediment at the subglacial bed, possibly enhanced by bed strength variations in response to heterogeneities in till thickness and rheology, effective pressure and meltwater drainage (Clark, 2010; Chapwanya et al., 2011; Sergienko and Hindmarsh, 2013; Fowler and Chapwanya, 2014; Fannon et al., 2017).

In conclusion, ribbed bedforms occur in a highly varied distribution within ice sheets and ice streams and multiple

180   hypotheses have been proposed for their formation. A size and shape continuum has been observed between ribbed, hummocky and streamlined bedforms, suggesting that these subglacial bedforms could form in response to the same governing processes modulated by either ice flow velocity or ice flow duration (Aario, 1977; Rose, 1987; Dunlop and Clark, 2006b; Stokes et al., 2013a; Ely et al., 2016; Fannon et al., 2017). Moreover, ribbed bedforms are frequently embedded within polygenetic landsystems, corresponding to a multiphase story, which complicates their interpretation

185   (Cowan, 1968; Aylsworth and Shilts, 1989; Stokes et al., 2008). Previous studies emphasize the importance of ribbed bedforms in the reconstruction of basal shear stress, ice-bed interactions, basal processes and ice dynamics (Dyke and Morris, 1988; Alley, 1993; Sergienko and Hindmarsh, 2013; Sergienko et al., 2014).

3. Methods

3.1. Analog modelling

190   The development of subglacial bedforms potentially involves three processes – transport, deposition and deformation – that can occur simultaneously and interact beneath ice streams, and four components - ice, water, till, and bedrock – that have complex and distinct rheological behaviours (Paterson, 1994). To understand the formation of ribbed bedforms, numerical models have been developed using naturally-occurring typical values for the physical properties of these components. In these models the initiation of subglacial bedforms is based on (i) the development of along-flow

195   instabilities which creates wave-like bedforms resulting from infinitesimal perturbations at the surface of a viscous till layer (Hindmarsh, 1998; Fowler, 2000; Schoof, 2007; Chapwanya et al., 2011; Fowler and Chapwanya, 2014; Fannon et al., 2017), and (ii) till entrainment and deposition resulting from till flux (driven by bed deformation and ice pressure gradient) and lee-side cavity deposition (Barchyn et al., 2017). Three-dimensional numerical modelling of bedforms remains a challenging enterprise however, and investigation is far from complete, mostly because the involved

200   components show drastically distinct thermo-dependent and strain-rate dependent rheologies, and therefore temporal scales of activity (Paterson, 1994). To circumvent the challenge of numerically modelling these complex interactions, Lelandais et al. (2016, 2018) developed a physical laboratory model able to simulate simultaneously ice flow, subglacial hydrology and subglacial erosion/transport/sedimentation/deformation. This model contributed to better constrain the link between subglacial meltwater drainage and the lifecycle of ice streams, but subglacial bedforms did not arise. We used

205   the same approach with a new experimental setup, specifically designed to simulate the development of subglacial bedforms.

3.1.1. Experimental setup

The experimental device consists in a stainless steel box, 5 cm in depth and 2 m × 2 m in horizontal size, surrounded by a gutter 5 cm in width (**Fig. 2a**). A 5 cm thick bed, composed of saturated fine sand (median grain size d_{med} = 100 μm,

210   density ρ_{bulk} = 2000 kg·m^{-3}, porosity Φ_s = 41 %, permeability K_s = 10^{-4} m·s^{-1}) fills the box to simulate a soft, porous, permeable and erodible subglacial bed (**Fig. 2b**). Grains of coloured coarse sand (grain size d = 850 to 1250 μm),

representing bedrock blocks, are sprinkled over the flat surface of the bed. To simulate the ice sheet, a circular cap of viscous and transparent silicon putty (density ρ_{sil} = 967 kg·m^{-3}, viscosity η_{sil} = 5.10^4 Pa·s^{-1}), 3 cm thick in its centre and 90 cm in diameter, covers the bed. We inject a solution of mixed water and UV ink (bulk density ρ_w = 998 kg·m^{-3}) through

215 an injector located below the centre of the silicon cap in order to produce water flow beneath the silicon and highlight the flow pattern using UV light. The central injector, with a diameter of 8 mm, is placed 1.5 cm beneath the surface of the bed and supplied by a water pump. The injection discharge is regulated by a flow meter (discharge Q = 0-50 ml·min^{-1}) and is calculated to allow water circulation within the bed and along the silicon-bed interface, with a pressure of injected water exceeding the combined weights of the bed and silicon layers.

220 Fifteen experiments, 60 min in duration, were performed with different injection scenarios: constant, binary and discontinuous (**Table 1**). The experimental device is scaled according to the principles described in Lelandais et al. (2016, 2018): to take into account the intimate links between glacial dynamics, subglacial hydrology and subglacial landform development, all physical quantities in the experiment are defined so that the dimensionless ratio between ice velocity and incision rate of subglacial erosional landforms has similar values in the model and in nature. Lelandais et al. (2016,

225 2018) demonstrated that models based on this scaling ratio are able to reproduce landforms representative of subglacial systems.
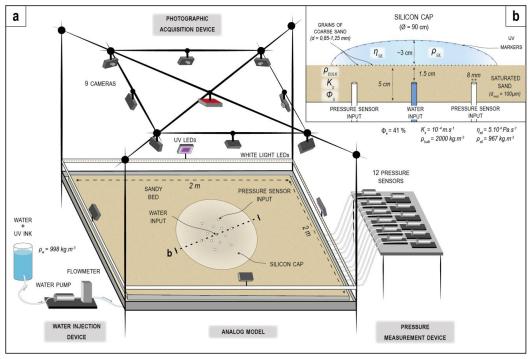

Figure 2. (a) Scheme of the experimental model and monitoring apparatus. A cap, of transparent and viscous silicon putty, flows under its own weight above a bed composed of water-saturated sand. We inject coloured water in the bed, through an
230 **injector located below the centre of the silicon cap. We used a photographic acquisition device and pressure sensors to monitor the development of bedforms at the silicon/bed interface, the silicon flow velocity, the water flow and the water pressure. (b) Transverse section of the model with the experimental parameters.**

3.1.2. Monitoring of experiments and post-processing of data

The experimental device is equipped with white light LEDs and UV LEDs, alternating every 15 seconds during an
235 experiment. An array of nine cameras acquires photographs (every 15 seconds) both in white light (all cameras) and in

UV light (red camera only; **Fig. 2a**). The transparency of the injected water and the silicon cap in white light enables manual mapping of bedforms and reconstruction of Digital Elevation Models (DEMs) of the bed surface from the white light photographs, with a precision of ± 0.1 mm, through a photogrammetric method developed by Lelandais et al. (2016). The morphometric properties of bedforms and drainage features (**Fig. S1**) are calculated from interpreted snapshots and

240 DEMs. Maps of water distribution at the silicon-bed interface are derived from the UV photographs, thanks to the fluorescence of the injected water. An automatic treatment of these images and a calibration with DEMs of the sub-silicon bed allows fluorescence intensity to be converted into water thickness. The pore-water pressure is measured, 1.5 cm beneath the bed surface, with twelve pressure sensors (8 mm in diameter) distributed in two concentric circles, 15 and 30 cm in radius respectively and centered on the central water injector (**Figs. 2a, b**). The horizontal positions of UV markers,

245 1 mm in diameter and placed with an initial spacing of 5 cm on the silicon surface, are monitored with a time step of 90 s (**Fig. 2b**). Horizontal velocity (V_{surf}) and deformation maps for the surface of the silicon cap are then calculated and interpolated from the temporal record of the marker displacements. The horizontal deformation of the silicon cap surface is quantified with three indicators, (i) the rotation angle (α) and (ii) elongation (L_R) of the horizontal strain ellipse (Ramsay & Huber, 1987), and (iii) the absolute magnitude of the horizontal shear strain rate (ε_{shear}; Nye, 1959). Those indicators

250 are computed for each triangle of a mesh, established by a Delaunay triangulation of all the UV markers (**Fig. S2**).

Experiment number	Water injection scenario	Channelized drainage beneath lobes	
		Well-developed	Poorly-developed
1	Constant 25 ml·min⁻¹ (60 min)	■	
2		■	
3		■	
4		■	
5		■	
6	Constant 37.5 ml·min⁻¹ (60 min)	■	
7			■
8		■	
9			■
10	Binary 25 ml·min⁻¹ (30 min) - 50 ml·min⁻¹ (30 min)	■	
11		■	
12		■	
13	Discontinuous 12.5 ml·min⁻¹ (15 min) - 25 ml·min⁻¹ (15 min) - 0 ml·min⁻¹ (15 min) - 25 ml·min⁻¹ (5 min) - 37.5 ml·min⁻¹ (5 min) - 50 ml·min⁻¹ (5 min)	■	
14			■
15		■	

Table 1. Water injection scenarios and type of water drainage observed in each experiment.

3.2. Mapping and morphometric analysis on paleo-ice stream landsystems

To identify, map and characterize ribbed bedforms associated with natural palaeo-ice stream edges, we compiled Digital Elevation Models (DEMs), hillshades and ice stream contours of the North American Laurentide Ice Sheet (Margold et

255 al., 2015) in a Geographic Information System. Four distinct regions (**Fig. 3**), covering a few thousand square kilometres, overlapping the shear and lobe margins of three palaeo-ice stream beds were studied: (i) the Amundsen Gulf Ice Stream (21.8 – 12.9 cal ka BP), (ii) the Central Alberta Ice Stream (20.5 – 17 cal ka BP) and (iii) the Hay River Ice Stream (13.9 – 12.9 cal ka BP; Margold et al., 2018). We used a 15 m LiDAR bare-earth DEM supplied by the Alberta Geological Survey for the Central Alberta and Hay River ice streams, and a 10 m Digital Surface Model computed by optical stereo

260 imagery (ArcticDEM; Porter et al., 2018) for the Amundsen Gulf Ice Stream. By means of break in slopes observed on

hillshades, we digitized ribbed bedforms, streamlined bedforms indicative of predominant ice flow directions and other landforms indicative of ice stream lateral and frontal margins at the scale 1:50 000. The length (long-axis), width (short-axis) and orientation of ribbed bedforms compared to ice flow direction were extracted using the 'Minimum Bounding Geometry' tool in ArcGIS. The orientation values of ribbed bedforms and streamlined bedforms were compiled in rose
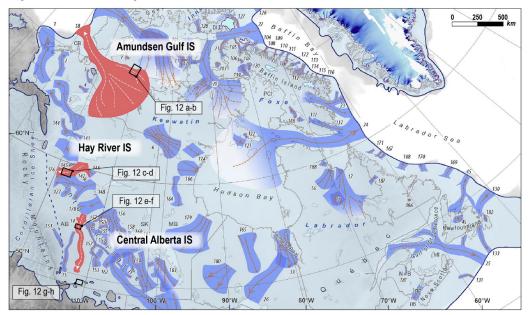265 diagrams for each selected region.

Figure 3. Extent of the North American Laurentide Ice Sheet during the Last Glacial Maximum with positions of known ice stream tracks (modified from Margold et al., 2018). The areas mapped in this study are identified by black rectangles in three ice streams (Amundsen Gulf, Hay River and Central Alberta IS).

270 **4. Results**

4.1. Ice stream dynamics and development of ribbed bedforms in the experiment

Without evident link with the distinct experimental setups, the experiments listed in **Table 1** produced two types of streams and lobes related to two different kinds of water drainage networks beneath the silicon cap: (i) a well-developed channelized drainage (n = 12 experiments) and (ii) a poorly-developed channelized drainage (n = 3 experiments). In the
275 following section, we present the evolution of silicon stream dynamics and ribbed bedforms for one experiment representative of each kind: experiments 10 and 14, respectively (**Table 1**). In those two experiments, the water injection was doubled in stage 3 ($Q = 50$ ml·min^{-1}) compared to stages 1 and 2 ($Q = 25$ml·min^{-1}).

In both experiments, when water injection starts, a circular water pocket forms and grows along the silicon-bed interface until it reaches a diameter of 15 to 25 cm. This pocket migrates towards the margin of the silicon cap, as a continuous
280 water film, until it suddenly drains outside the cap. The presence and migration of the water pocket induces a local increase in silicon flow velocity (from $V_{surf} = 0.2 \times 10^{-2}$ mm·s^{-1} to $V_{surf} = 10 \times 10^{-2}$ mm·s^{-1}) forming a 20 cm wide stream that propagates from the margin towards the centre of the silicon cap. A lobe forms at the extremity of the fast-flowing corridor in response to this drainage and surge event. In Experiment 10, seven water pockets successively form and produce as many drainage events and lobe advances; in Experiment 14, only one drainage event occurs (**Fig. 4**). The drainage events
285 generate marginal deltas along the silicon margin, constituted by sand grains eroded from the bed during the migration of

the water pocket. The sustainability of a water film at the silicon-bed interface, once the initial drainage event is over, contributes to maintain a fast and durable silicon flow, the silicon stream switches on and the silicon lobe keeps growing. Landforms produced in the experiments are illustrated and annotated in **Fig. 5**: these include grooves, ribbed and hummocky bedforms beneath the streams, and marginal deltas and pushed sediments in front of the lobe. The successive stages (**Figs. 6 to 9**) are described below in relation to: (i) the stream evolution derived from surface measurements of their kinematics, (ii) the formation, evolution and the morphometric characteristics of bedforms derived from photographs in white light and DEMs, and (iii) the evolution of water drainage systems derived from UV photographs and DEMs.

Figure 4. Evolution of pore water pressure (solid lines) measured in the trunk axis (see Fig. 5a for position) and water flow injected in the bed through the water injector (dotted lines), for Experiments 10 and 14. Points numbered 1 to 3 correspond to stages described in sections 4.1, 4.2 and 4.3.
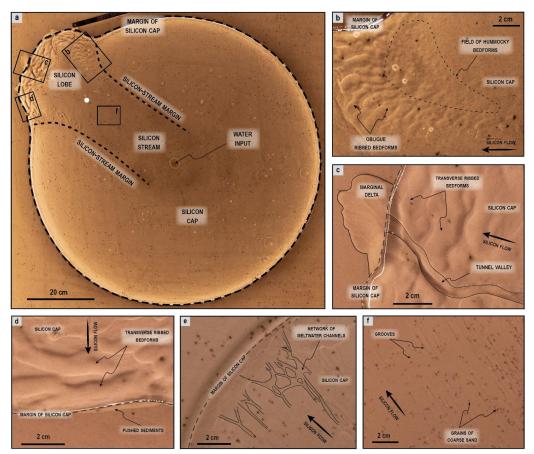

Figure 5. Illustration of bedform assemblages produced during the experiments. (a) Overall surface view of the silicon cap at the end of an experimental run, showing the distribution of bedforms beneath a stream/lobe system characterized by a well-developed channelized drainage (Experiment 10). The white dot indicates the position of the pressure sensor where pore water

pressure presented in Fig. 4 is measured. **(b)** Close-up on oblique ribbed and hummocky bedforms observed at the right lateral trunk margin. **(c)** Transverse ribbed bedforms parallel to the lobe margin and formed submarginally. Tunnel valley and associated marginal delta. **(d)** Transverse ribbed bedforms parallel to the lobe margin and pushed marginal sediments bulldozed by the lobe margin. **(e)** Network of meltwater channels extending parallel and perpendicular to the silicon flow (not located on (a), because it was observed in Experiment 14, characterized by a poorly-developed channelized drainage). **(f)** Field of grooves inscribed in the bed and oriented parallel to silicon flow with embedded sand grains at their down-stream extremities.

4.1.1. Stage 1 - Initiation of ribbed bedforms beneath incipient shear and lobe margins

The streams flow ten to twenty times faster (**Fig. 7a**: $V_{surf} = 0.08$ mm·s^{-1}; **Fig. 9a**: $V_{surf} = 0.17$ mm·s^{-1}) than the inter-stream areas ($V_{surf} < 0.01$ mm·s^{-1}), inducing velocity gradients across the lateral margins of the streams. The rotation angle of the strain ellipse and the shear strain rate are zero in the centre of the stream trunk and in the surrounding ice cap, while they are maximal along lateral margins of the streams where the velocity gradient is the highest (**Figs. 7a, 9a**; α = up to 8°; L_R = 15-20%; ε_{shear} = 3 to 5×10^{-4} s^{-1}). These patterns of high shear deformation define symmetrical bands on the silicon surface, and resemble those of natural shear margins (Echelmeyer et al., 1994; Raymond et al., 2001).

In experiment 10 (**Fig. 7a**), the stream velocity decreases from the centre ($V_{surf} = 0.08$ mm·s^{-1}) toward the frontal and shear margins (respectively, $V_{surf} = 0.06$ mm·s^{-1} and $V_{surf} = 0.04$ mm·s^{-1}), while the silicon-bed interfaces of these margins are dewatered (**Fig. 7a**; water thickness = 0). Beneath the lobe, meltwater channels, 50 to 70 mm in length and 4 to 8 mm in width, start to develop eroding progressively upstream from the margin and initiate channelization of the water flow (**Figs. 6a, 8a**). Sand grains washed away by bed erosion are transported within these incipient channels towards the marginal deltas (**Figs. 5c, 6a**). Radial growth and advance of these lobe over the marginal deltas form ridges of pushed sediments, 5 mm in width and 40 mm in length (**Figs. 5d, 6a**). Below the streams (**Fig. 6a, 8a**), some coarse sand grains are lodged in the base of the fast-flowing silicon and carve the bed to form sets of parallel grooves (1 mm wide, 10 to 20 mm long) highlighting the stream trunk and the direction of the silicon flow (**Figs. 5f**). Below frontal and shear margins, fields of periodic ridges develop transverse to ice flow, with undulating crests and an average wavelength of 8 mm (**Figs. 6a, 8a**). They are on average a few millimetres thick, 7 mm wide and 30 mm long, i.e. 4 times larger in length than in width. Their shapes (undulating crest, elongation ratio) and spatial organization (periodicity) (**Figs. 5b, d**) are similar to those of ribbed bedforms observed in glacial landsystems. In the experiments, most of the ribbed bedforms initiate almost parallel to the lobe margins and perpendicular to the silicon flow direction, but some scattered and isolated ribbed bedforms arise oblique (50°) to silicon flow. Other bedforms with circular to ovoid shapes (mounds) form close to the ribbed bedforms. These mounds are typically less than 0.1 mm high, 4 mm wide and 6 mm long, with an average spacing of 10 mm. Their long-axes do not show a preferential orientation (**Figs. 6a, 8a**). The shape and spatial organisation of these mounds (**Fig. 5b**) are similar to those of hummocky bedforms in glacial landsystems.

4.1.2. Stage 2 – Channelization of the drainage system below protruding lobes and evolution of ribbed bedforms

After half an hour, channelized networks develop beneath the silicon lobe, draining water fed from the upstream water film towards the margin. The morphological evolution of these networks differs between both types of experiments, and we suggest is a controlling influence on the distinctive evolution of stream dynamics from this point. From the previous stage, the incipient network of meltwater channels in Experiment 10 evolved into tunnel valleys (**Fig. 5c**), increasing in width (up to 1.2 cm), length (15 cm) and depth (0.07 cm), and marginal deltas continued to grow (**Fig. 6b**). Three individual tunnel valley systems are observed (**Fig 6b**): two slightly sinuous valleys with some tributaries and one anastomosed valley network. Simultaneously, the stream velocity decreased by half, resulting in a slowdown in the advance of the lobe margin (**Fig. 6b**: 28 cm in width; **Fig. 7b**: $V_{surf} = 0.04$ mm·s^{-1}). Proportionally to the slowdown intensity, the shear margins record a halving of shear strain rate (**Fig. 7b**: $\varepsilon_{shear} = 1.25 \times 10^{-4}$ s^{-1}) and strain ellipse rotation (α = 4°; L_R = 10%).

In contrast to the above, in Experiment 14 the pre-existing meltwater channels remain shallow and keep a constant width,

345   but lengthen downstream in response to the migration of the lobe margin (**Fig. 8b**: 0.4 cm wide, 12 cm long, 0.04 cm deep). Meltwater channels are rectilinear with poorly developed tributaries and lack deltas at their downstream extremities (**Fig. 5e**). In parallel, the silicon stream flow maintains a high velocity, although a small deceleration occurs (**Fig. 9b**: $V_{surf} = 0.13$ mm·s^{-1}), sustaining lobe growth (36 cm in width). As a result, the shear margins record a small decrease of the shear strain rate (**Fig. 9b**: $\varepsilon_{shear} = 3.5 \times 10^{-4}$ s^{-1}) and a downstream-to-upstream increase of the rotation and elongation

350   of strain ellipses (α = up to 18°; L_R = up to 32%).
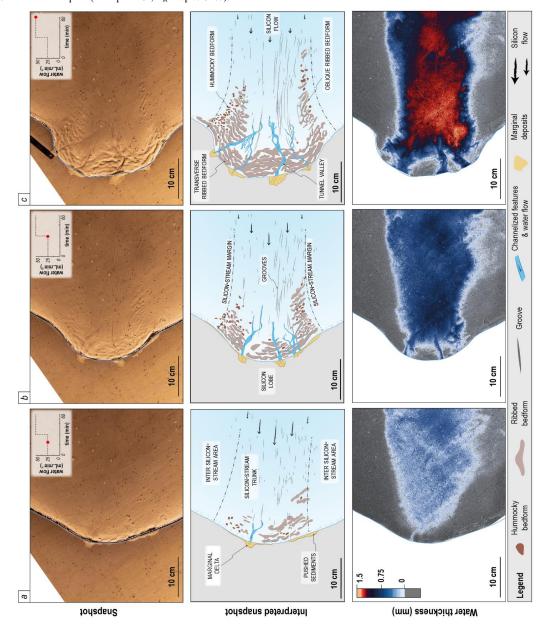

Figure 6. Temporal evolution (stages a, b and c) of the silicon stream and lobe system, for a typical experiment with a well-developed channelized drainage system (Experiment 10), illustrated with snapshots representative of the three main stages of development. The upper, intermediate and lower panels show, respectively, (i) white-light photographs of the surface of the

355   **model, (ii) interpretations of bedforms observed on the photographs and (iii) thickness (in mm) of the water film flowing beneath the silicon cap, derived from UV photographs.**
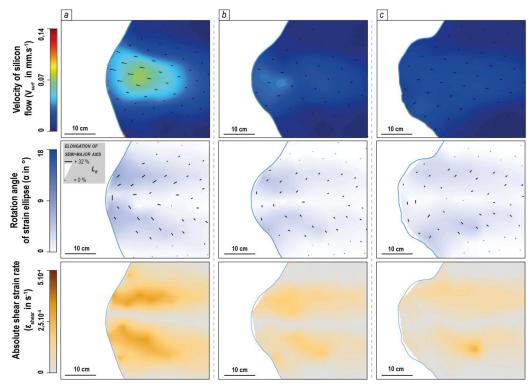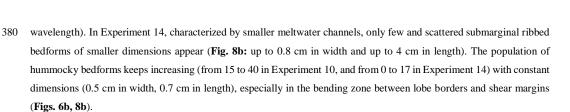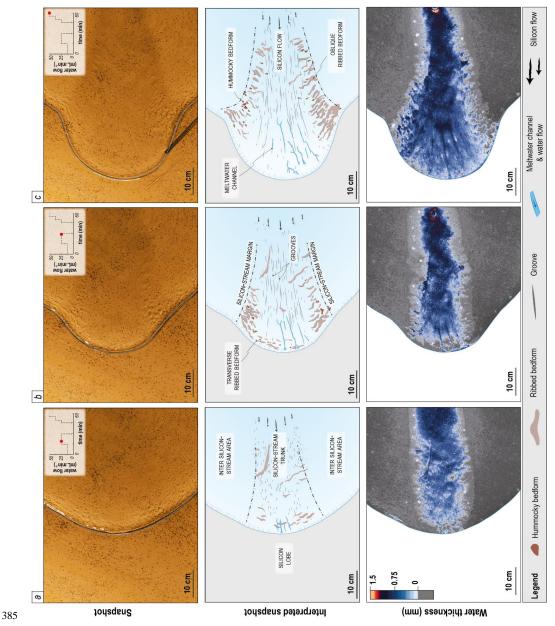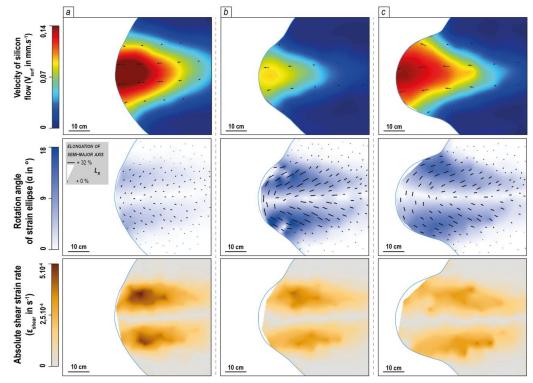

Figure 7. Temporal evolution (same stages a, b and c than Fig. 6) of the silicon stream and lobe system, for a typical experiment with a well-developed channelized drainage (Experiment 10). The upper, intermediate and lower panels show respectively, (i)
360   **the velocity field of silicon flow (mm·s^{-1}) and the displacement vector maps of the silicon cap upper surface, (ii) extrapolated maps of rotation angle of strain ellipse (α in °), elongation (L$_R$ in %) and orientation of semi-major axis, and (iii) extrapolated maps of absolute shear strain rate (s^{-1}). Maps highlight the development of the fast-flowing corridor (i.e. silicon stream) surrounded by stagnant or very slow-moving silicon (i.e. inter stream area) and the formation of two symmetrical shear bands on both sides of the stream (i.e. the shear margins).**

365   Within the trunk of both experiments, the orientation and direction of the grooves matches the direction and velocity of the silicon flow. The grooves are restricted to the fast-flowing corridor and display lengths up to 5 cm and 8 cm for Experiments 10 and 14 respectively, and they tend to keep a constant width of approximately 0.1 cm. Grooves remain rectilinear and parallel to mean flow direction in the upstream part of the streams but diverge and curve in the downstream area following the radial flow pattern of the lobe (**Figs. 6b, 8b**). During this second stage, the ribbed bedforms keep

370   growing but differ below shear (i.e. lateral ribbed bedforms) and lobes (i.e. submarginal ribbed bedforms) margins. Below shear margins, new lateral ribbed bedforms with arcuate planforms progressively develop, first appearing near the lobe and then toward the upstream area of the trunk borders. Pre-existing ribs increase in length and width (**Figs. 6b, 8b**; 1 cm wide and 5 cm long). Lateral ribbed bedforms become more oblique through time (up to 40° relative to the silicon flow direction). Their wavelength is typically 0.6 to 0.7 cm in Experiment 10 (**Fig. 6b**), while it is 1.0 to 1.5 cm in Experiment

375   14 (**Fig. 8b**). Beneath the lobe margin of Experiment 10, the water film ceases to exist in-between the tunnel valleys (**Fig. 6b**). These water-free areas coincide with the formation of submarginal ribbed bedforms parallel to the lobe margin. They develop below the lobe from (i) the initial sandy bed and (ii) the recycled marginal landforms (i.e. marginal deltas and pushed sediments). The development and the coalescence of these bedforms below the lobe tend to form a belt composed of broad, arcuate and transverse submarginal ribs (**Fig. 6b:** up to 1.6 cm in width, up to 8 cm in length and 1.1 cm in

380 wavelength). In Experiment 14, characterized by smaller meltwater channels, only few and scattered submarginal ribbed bedforms of smaller dimensions appear (**Fig. 8b:** up to 0.8 cm in width and up to 4 cm in length). The population of hummocky bedforms keeps increasing (from 15 to 40 in Experiment 10, and from 0 to 17 in Experiment 14) with constant dimensions (0.5 cm in width, 0.7 cm in length), especially in the bending zone between lobe borders and shear margins (**Figs. 6b, 8b**).

385

Figure 8. Temporal evolution (stages a, b and c) of the silicon stream and lobe system, for a typical experiment with a poorly-developed channelized drainage (Experiment 14). Same panels than Figure 6.

Figure 9. Temporal evolution (same stages a, b and c than Fig. 8) of the surface behaviour of the silicon stream and lobe system, for a typical experiment with a poorly-developed channelized drainage (Experiment 14). Same panels than Figure 7.

4.1.3. Stage 3 – Morphological response to changes in drainage characteristics

The two experimental runs described here – after 60 minutes – show distinctive drainage systems (well-developed vs. poorly-developed), silicon streams dynamics and landform development.

Well-developed channelized drainage system (Experiment 10)

Tunnel valleys – characterized by undulating long profiles with over-deepening and adverse slopes – increase in number (from 3 to 4) and in dimensions (up to 1.1 cm wide, up to 16 cm long and up to 0.10 cm deep) and keep ensuring the drainage of a distributed water film. Tunnel valleys continue to grow downstream, tracking advance of the lobate margin and they incise the belt of submarginally-produced ribbed bedforms formed during the previous stage, as indicated by elevation profiles (**Figs. 6c, 10a, d**). The silicon flow velocity decreases along the stream axis and lobe growth slows down (L_{stream} = 20 cm; V_{surf} = 0.02 mm·s^{-1}). In response to this slowdown, the lateral velocity gradient decreases across the stream margins, whose width becomes constant ($L_{shear\,margin}$ = 11 cm). In these areas, the rotation and elongation of the strain ellipse (α = 3-4°; L_R = 10%) and the shear strain rate (ε_{shear} = 1 × 10^{-4} s^{-1}) stabilize at low values even if the rotation of strain ellipses increases downstream (**Fig. 7c**). The DEM displays submarginal ribbed bedforms evolving in a curved belt with a normal (90°) to subnormal (70°) orientation to the silicon flow in response to the radial flow pattern in the lobe (**Fig. 10, 11c**). Individual submarginal ribbed bedforms increase in dimensions and tend to evolve into a roughly coalescent belt (**Figs. 10c**; 1.4 cm in width, 4.2 cm in length and 0.1 cm in height), although they still display a regular wavelength, from 1.0 to 1.5 cm. New lateral ribbed bedforms form upstream below shear margins, while pre-existing ones tend to become more oblique to the local silicon flow and increase in dimensions. Elevation profiles reveal they remain smaller and display lower relief than their submarginal counterparts (**Figs. 10e**; 2.3 cm in length, 0.7 cm in width

and up to 0.07 cm in height). Lateral ribbed bedforms display a regular and oblique pattern, with most of the orientation

values comprised between 60° and 30° to local silicon flow (**Fig. 11c**) and a wavelength close to 0.7 cm (**Fig. 6c**).

Figure 10. DEMs of the bed surface beneath the lobes of the silicon streams at the final stage of experiment 10 (blue) and 14
415 (brown). Ten elevation profiles (a to e) within the lobes are drawn to compare the morphological imprint beneath the two types
of streams.

The grooves still increase in length, but at a slower rate than during previous stages, although remaining parallel (0°) or

subparallel (10°) to the silicon flow direction (**Fig. 11c**). The position and length of the grooves correlate with the time-
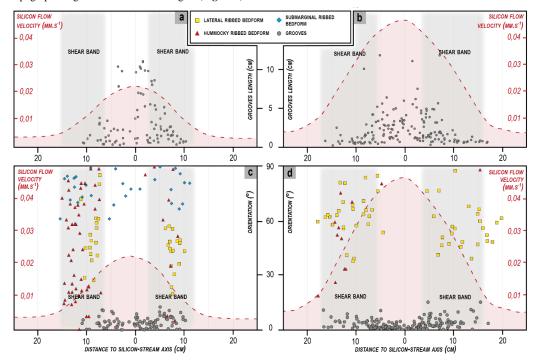
averaged velocity profile measured across the silicon stream (**Fig. 11a**). Hummocky bedforms occur either sparsely

420 between lateral ribbed bedforms or more densely in lobe corners. Their average length is 0.6 cm and their average width is 0.4 cm (**Fig. 6c**).

Poorly-developed channelized drainage system (experiment 14)

In response to the increase in water discharge, the sparse, shallow and narrow meltwater channels characterized by smoothly undulating long profiles (**Figs. 10a, d**; n = 9, up to 0.5 cm in width and up to 0.05 cm in depth) are not able to

425 evacuate all the water transmitted to the bed. Thus, the distributed water film, hitherto constrained to the uppermost part of the stream, spreads down to the lobe (**Fig. 8c**). The stream velocity increases and the lobe undergoes a surge (**Fig. 9c**; V_{surf} = 0.15 mm·s⁻¹). The high velocity gradient between the stream and the inter stream area maintains a high rate of deformation of the silicon along the shear margins, with a strain ellipse rotation increasing downstream (α = up to 18°; L_R = 25%) and a maximal value of shear strain rate localized along stream borders (ε_{shear} = 3 × 10⁻⁴ s⁻¹). The shear margins

430 widen downstream, reaching a maximum width at the silicon cap margin within the lobe corners ($L_{shear\ band}$ = up to 20 cm). Simultaneously with the downstream migration of the water film, the submarginal ribbed bedforms are eroded and evolve into a single low and smooth submarginal relief slightly higher than the trunk (**Fig. 10c**). The lateral ribbed bedforms keep increasing in number (from 26 to 42) and in dimensions (**Figs. 8c, 10e**; 3.6 cm in length, 1.1 cm in width and up to 0.09 cm in height). Located beneath the shear margins, they are characterized by subnormal to oblique long-

435 axes, deviating by 80 to 40° from the local silicon flow direction (**Fig. 11d**). Elevation profiles show that the ribbed bedforms are spaced with a wavelength comprised between 1.5 and 1.9 cm (**Fig. 10e**) and develop on both sides of a flat and grooved trunk (**Fig. 10c**). The corridors of lateral and oblique ribbed bedforms thus constitute two bands of topographic highs below the shear margins (**Fig. 10b**).

440 **Figure 11. Morphometric properties of bedforms produced beneath each type of stream at the final stage of Experiments 10 (right panel) and 14 (left panel) plotted according to the distance from the silicon stream central axis. (a) and (b) relationship between groove length and silicon flow velocity (mm·s⁻¹). (c) and (d) variation in orientation of each population of bedforms (lateral ribs, submarginal ribs, hummocky) compared to the silicon flow velocity and the shear band position (grey columns; defined as ε_{shear} > 0.5 s⁻¹).**

445   The grooves are more elongated near the trunk axis where the highest flow velocities are recorded, than near the shear margin where the velocity decreases (**Fig. 11b**). Following the radial spreading of the silicon flow towards the lobate margin, the groove orientations curve and form a fan-shaped swarm (**Fig. 8c**). Groove orientations mostly remain parallel to subparallel to the local silicon flow however, with a maximum deviation of 15° from the silicon flow direction (**Fig. 11d**). Sparse hummocky bedforms (width = 0.6 cm; length = 1.0 cm) occasionally occur within the corridors of lateral
450   ribbed bedforms.

4.2. Palaeoglaciology: ribbed bedforms beneath ice stream margins

Palaeo-ice stream trunks of the Laurentide Ice Sheet – both with marine (**Figs. 12a-b**) and terrestrial margins (**Figs. 12c-h**) – are characterized by dense swarms of streamlined bedforms (e.g. mega scale glacial lineations, drumlins), evidencing former ice flow directions. Their lateral margins– already identified by Margold et al. (2015) – are recognized through
455   sharp transitions in streamlined bedform zonation, topographic borders, shear moraines and marginal bedforms. In total, we mapped 303 ribbed bedforms in four distinct areas on three palaeo-ice stream beds.

In the eastern branch of the marine-based Amundsen Gulf Ice Stream (AGIS), two fields of ribbed bedforms (n = 62) elongated oblique to the ice flow direction occur along the lateral margins. The trunk is characterized by streamlined bedforms delimited by two topographic borders. In the northern margin, the long-axes of ribbed bedforms are oblique to
460   the ice flow direction (mean orientation = 45°), while in the southern margin they tend to be almost aligned to the streamlined bedforms (mean orientation = 25°). The ribbed bedforms display elongated and arcuate shapes (l/w = 4.2; mean length = 4780 m; mean width = 1110 m), and display a mean wavelength of 1450 m (**Figs. 12a-b**).

In the northern portion of the Hay River Ice Stream (HRIS), broad arcuate to rectangular ribbed bedforms (n = 78) strike oblique to the local ice flow direction. The ridges are clustered in an elongated corridor located between the northern
465   shear margin and the swarm of streamlined bedforms. The shear margin is marked by topographic borders, a sharp transition between a rough inter-ice stream terrain and a smooth trunk covered by lineations, and linear ridges similar to shear moraines. The ribbed bedforms exhibit a mean orientation of 55° to ice flow direction and a mean wavelength of 460 m. Those ridges are shorter (1040 m in length and 360 m in width) and slightly less elongated (l/w = 2.9) than those of the AGIS (**Figs. 12c-d**).

470   In the upstream portion of the Central Alberta Ice Stream (CAIS), oblique and transverse ribbed bedforms (n = 71) are also recognized. Similar to the AGIS and HRIS, the ice stream trunk is characterized by topographic borders, a smoother bed than the surrounding landscape, a meltwater channel and a swarm of lineations. The ribbed bedforms located to the east of the meltwater channel are superimposed by lineations, while the oblique ribbed bedforms along the ice stream margins are apparently not overprinted by other structures. The ribbed bedforms display orientations ranging from 15 to
475   25° to ice flow direction for the slightly oblique set, while the transverse set displays orientations deviating by 85°. They are 2660 m in length and 690 m in width – thus displaying a mean elongation ratio of 3.8 – and have a mean wavelength of 685 m (**Figs. 12e-f**). The oblique ribbed bedforms are characterized by less arcuate and more elongated shapes than the transverse ones. Downstream and further south in the CAIS, is a widespread belt of transverse ribbed bedforms (n = 92; mean orientation = 95°) overprinted with perpendicular lineations and cross-cut by large meltwater channels (width
480   = 0.6 to 3.4 km). This belt presents a regular pattern of arcuate and coalescent ribbed bedforms (wavelength = 600 to 1 200 m), paralleling a curved belt of fine, linear and almost continuous ridges – similar to recessional moraines – depicted further north. The mean length (4350 m), width (1350 m) and elongation ratio (l/w = 3.0) of the ribbed bedforms show that these ridges are longer, wider but less elongated than the oblique and transverse ridges upstream (**Figs. 12g-h**).
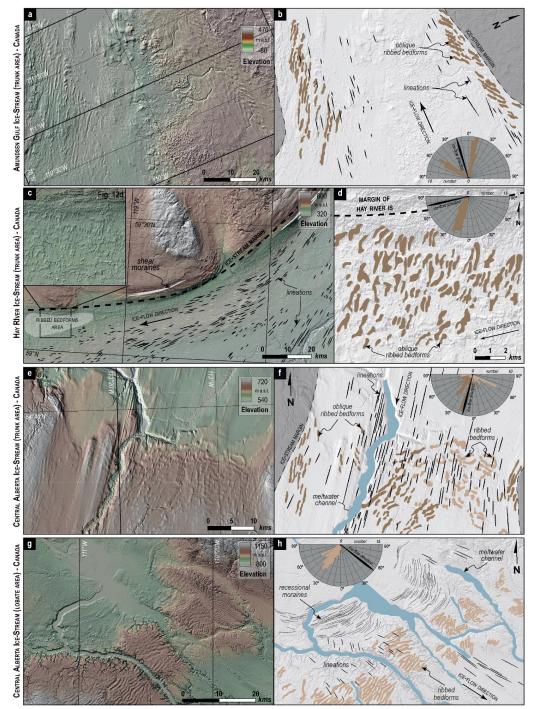
485

Figure 12. Manual mapping of ribbed bedforms, lineations and ice stream margins along different palaeo-ice stream tracks in Canada. Left panels show digital elevation models and hillshades using Arctic DEM database (Porter et al., 2018) and Lidar data (Alberta Geological Survey). Right panels show our morphological interpretations and the rose diagrams compiling bedform orientations.

5. Discussion

5.1. Comparison between experimental and natural ribbed bedforms

Through experimental modelling and landform mapping, we observed the occurrence of ribbed bedforms beneath the shear (i.e. lateral ribs) and lobe (i.e. submarginal ribs) margins of ice streams. They are found to be clustered in corridors and belts below zones displaying transverse and longitudinal velocity gradients respectively. The ribbed bedforms are mostly observed along the borders of swarms of elongated structures (**Figs. 6, 8, 12**; i.e. lineations in nature and grooves in the experiments) that reveal fast-flowing ice stream trunks (Stokes & Clark, 2001; Clark & Stokes, 2003). Beneath the shear margins of the experimental ice streams, the lateral ribbed bedforms have transverse-to-oblique long-axes (**Figs. 10c-d**; mean orientation = 30 to 80°) and tend to gather in corridors elongated parallel to the ice flow direction. In the experiments, their elongation ratio of 3.3 (mean length = 2.95 cm; mean width = 0.90 cm) lies in between those of natural traction ribs and mega-scale transverse ridges, fitting a moderately elongated type of ribbed bedforms. The submarginal ribbed bedforms generated below lobe margins have a mean elongation ratio of 3.0 (mean length = 4.2 cm; mean width = 1.4 cm) and a mean long-axis almost perpendicular to the local silicon flow (mean deviation = 80-90°). Our observations of ribbed bedforms developing diagonal to flow in the physical experiments suggests that this might also occur in nature, and examples have been noted such as in traction ribs (Stokes et al., 2016) and diagonal banding (i.e. partially drumlinized ribbed bedforms) found in drumlin spatial organisation (Greenwood & Clark, 2008; Clark et al., 2018). Along the shear margins of natural palaeo-ice stream beds, we mapped lateral ribbed bedforms whose long-axes display oblique orientations (15° to 55°) to the ice flow direction along palaeo-shear margins (**Figs. 12a-f**), while they tend to display a transverse orientation (~90°) close to lobe margins (**Figs. 12g-h**). Those lateral ribbed bedforms have medium elongation ratios (l/w = 2.9 - 4.2), and display an arcuate shape and a regular pattern. Along the shear margins of the AGIS (**Figs. 12a-b**), the obliquity of lateral ribbed bedforms was hitherto interpreted as converging generations of (downstream-aligned) streamlined bedforms, and thus as distinct flow sets arising from a change in flow direction over time (Winsborrow et al., 2004; Stokes et al., 2006; De Angelis & Kleman, 2007). If it is common for ribbed bedforms to arise diagonal to ice flow, then this needs careful consideration when using mapped bedforms to plot former ice flow directions such as in flow sets. We suggest that in the AGIS (**Figs. 12a-b**), that rather than separate flow sets, these landforms were generated in a single phase under unidirectional flow. An additional argument here is with regard to the elongation ratio obtained from the ridges mapped in this study (l/w = 4.2), and compared to the usual and much higher elongation ratio of mega-scale glacial lineations (l/w = 8.7; Stokes et al., 2013a). Similarly, even though they did not interpret their orientations, Greenwood and Kleman (2010) suggested that these bedforms could correspond to wavy transverse bedforms (l/w = 5.7). Furthermore, Sergienko & Hindmarsh (2013) and Sergienko et al. (2014) deciphered rib-like patterns of very high basal shear stress, driven by low hydraulic conductivity, beneath some modern ice streams (e.g. Pine Island Glacier or North-East Greenland Ice Stream). Rib-like features show clear oblique orientations and symmetrical distribution below the shear margins with angles deviating from 20 to 70° to the ice flow direction (**Fig. 13**), comparable to the lateral ribbed bedforms depicted in the AGIS (**Figs. 12a-b**). Regarding the CAIS, the ridges mapped in the upstream (trunk) and downstream (lobe) areas (**Figs. 12e-h**) were previously interpreted as traction ribs (Stokes et al., 2016) and overridden thrust masses (Evans et al., 2008, 2014; Atkinson et al., 2018) respectively. For both cases (i.e. trunk and lobe positions), we find the exceptional regularity in wavelength, form and scale between ridges to be suggestive of a common rather than entirely separate origin.
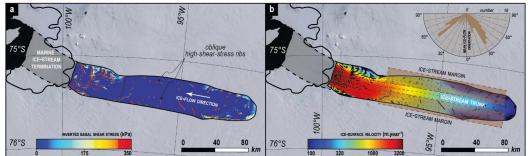
Considering their common spatial patterns, orientations, elongations and locations, we suggest that the ribbed bedforms (i) reproduced through experimental modelling and (ii) highlighted in our mapping within palaeo-ice stream beds are analogous and essentially the same thing. They occur below shear and lobe margins in places experiencing sharp spatial

gradients in ice velocity, and according to the samples measured thus far they tend to represent ribbed bedforms with a medium elongation ratio. Our suggestion of commonality of type and process of these landforms is preliminary and could be tested by field investigation and ideas developed regarding their formation processes which are still poorly constrained.

Figure 13: Maps of inverted (a) basal shear stress (kPa) beneath Pine Island Glacier and (b) ice-surface velocity (modified from Sergienko and Hindmarsh, 2013). Small and isolated areas of very high basal shear stress (red on (a) and black on (b)) reffered to as "high-shear-stress ribs" are obliquely set to the main ice flow direction . The orientations of oblique ribs relative to mean ice-flow direction, located in the brown rectangular areas (along ice stream margins), are compiled in a rose diagram in (b) (© Landsat / Copernicus - © Google Earth).

5.2. Processes of ribbed bedform formation at ice stream margins

We suggested that ribbed bedforms can form below shear and lobe margins of ice streams, areas with high velocity gradients (Echelmeyer et al., 1994; Patterson, 1997; Raymond et al., 2001). As observed in some of their natural counterparts, we experimentally demonstrated that shear margins can develop in response to sustained fast ice flow generated by surging events and lubrication of the silicon-bed interface (Dunse et al., 2015; Schellenberger et al., 2017; Lelandais et al., 2018; Sevestre et al., 2018; Zheng et al., 2019). In the light of the results of experimental modelling, we now propose a process of formation for the type of ribbed bedforms presented in this study that takes into account their morphology, the overlying ice dynamics and the subglacial hydrology.

5.2.1. Lateral ribbed bedforms below shear margins

Bougamont et al. (2011) and Tulaczyk et al. (2000) proposed that the formation of a shear margin can be entirely controlled by the subglacial hydrology if the bed properties and the ice thickness remain constant. According to our experiments, we suggest a similar behaviour: the lateral transition between the widespread and pressurized water film (**Fig. S3**) in the trunk that induces ice-bed decoupling and the dewatered outer area that induces ice-bed coupling, generates a stress balance disequilibrium (**Fig. 14**). In this configuration, the decrease of the basal drag in the trunk area induced by widespread decoupling has to be accommodated by an increase in lateral drag responsible for the formation of shear margins. The width of shear margins relative to that of the trunk is much higher in the experiments than their natural counterparts because the silicon, a Newtonian material, is unable to localise viscous deformation or to produce brittle deformation (by formation of crevasses for example) in the range of experimental flow velocities we can simulate. Based on our experiments, we suggest that ice along the shear margins flows – although it lies above a dewatered and coupled ice-bed interface – by simple shear because it accommodates a high velocity gradient (**Fig. 14**). The combination of ice-bed coupling and medium ice flow velocity (compared to the stream and the outer-stream areas) generates a high basal shear stress below the shear margins along the ice-bed interface. The basal shear stress could be periodically accommodated (i) by plastic bed deformation or (ii) by granular flow and sediment accretion in a basal soft bed, both resulting in the genesis of regularly-spaced ribbed and hummocky bedforms (**Fig. 14**). The water film spreads between

21

the incipient ribbed bedforms to form a linked-cavities system separated by ridges whose crests remain coupled to the

565 overlying ice (**Fig. 14**). Being coupled to the ice, the crest of ribbed bedforms keeps accommodating basal shear stress. As a result of continuous deformation and flow by simple shear, the strain ellipse in the ice elongates and rotates obliquely to the ice flow while the shear strain rate increases (**Fig. 14**). Given that incipient lateral ribbed bedforms develop beneath the shear margins, they record a continuous growth and a progressive rotation and elongation obliquely to the main direction of ice flow. Due to the specific stress and strain configuration, lateral ribbed bedforms developing beneath shear

570 margins of ice streams should present higher elongation ratios than the classic ribbed/Rogen moraines that occur outside ice stream contexts.
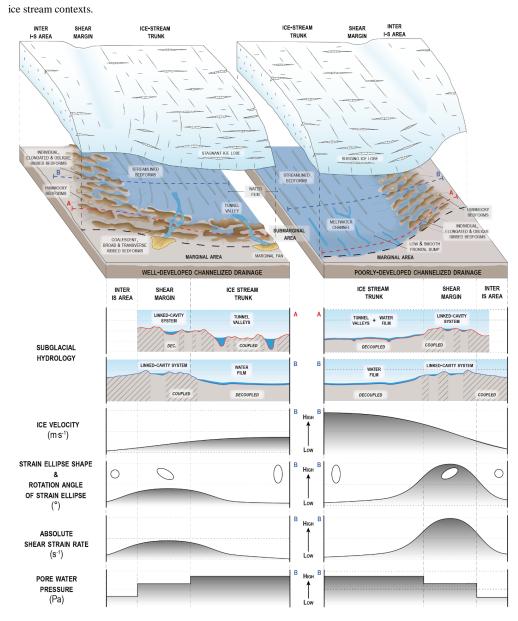

Figure 14. Conceptual model summarising our observations and interpretations and the proposed role of hydrology, ice velocity and subglacial shear in generating the observed landforms and their spatial distribution. This is for a terrestrial ice-stream

575 **context either characterized by well-developed or poorly-developed channelized drainage below the lobe frontal margin.**

5.2.2. Submarginal ribbed bedforms below lobe margins

Beneath lobe margins, the water film channelizes into a system of a well-developed tunnel valleys resulting in basal coupling and high basal shear stress in interfluve areas (**Fig. 14**). This reduction in basal lubrication leads to a slowdown in margin advance, a stabilization of the ice lobe and a downstream increase of longitudinal compressive stress. Similarly to the formation of lateral ribbed bedforms, the high basal shear stress below lobe margins could be periodically accommodated by the bed through (i) plastic deformation or (ii) granular flow, both leading to the formation of submarginal ribbed bedforms. Once initiated, the submarginal ribbed bedforms continuously grow and elongate perpendicular to the longitudinal compressive stress (i.e. parallel to the lobe margin) and a linked-cavities system develops in between the set of coalescent submarginal ridges (**Fig. 14**). We demonstrate that belts of coalescent ribbed bedforms mirroring the shape of lobe margin can also form subglacially in the distal part of ice streams. Similar coalescent ridges close to lobe termination have been hitherto interpreted as landforms resulting from the bulldozing of proglacial sediments or the subglacial remoulding of former marginal landforms during ice-lobe re-advances (e.g., glaciotectonic thrust masses, overridden moraines and push moraines for examples) (Totten, 1969; Boulton, 1986; Benn and Evans, 2010; Evans et al., 2014). We here propose an in-situ formation of ribbed bedforms resulting from the shearing of the subglacial bed (i.e., till layer or weak bedrock) beneath ice stream lobes.

5.2.3. Comparison with pre-existing model of ribbed bedforms formation

The consistent wavelength of natural and experimental ribbed bedforms described in this paper and their similarity in form and scale supports a single model of formation associated to high basal shear stress at the ice-bed interface, along zones undergoing high gradients of ice velocity (i.e. shear and lobe margins). Below modern ice streams (**Fig. 13**), Sergienko and Hindmarsh (2013) and Sergienko et al. (2014) deciphered rib-like patterns of very high basal shear stress with transverse and oblique orientations, whose morphological expression along palaeo-ice stream beds has been defined as traction ribs by Stokes et al. (2016). Our results demonstrate that such patterns of high basal shear stress could also be revealed by the formation of oblique and transverse ribbed bedforms below shear and lobe margins, respectively. Consequently, we suggest that these bedforms represent self-organized patterns resulting from the accommodation of high basal shear stress, either by (i) plastic deformation or (ii) sediment flow and accretion. These two hypotheses are consistent with other models which suggest that ribbed bedforms develop by either (i) folding, thrusting and stacking of basal till (Shaw, 1979; Aylsworth and Shilts, 1989) or pre-existing sediment layers (Lindén et al., 2008; Stokes et al., 2008), or (ii) flux of subglacial sediment/till driven by the ice flow and the shear stress along the basal interface (Stokes et al., 2013b; Barchyn et al., 2016). The contemporaneous development of ribbed bedforms and linked-cavities systems we observe in the experiments is consistent with the sedimentological work carried by Linden et al. (2008) who relates the development of ribbed bedforms to the deposition of sediments into the lee-side cavity of moraine ridges. Shear-heating within natural shear margins tends to produce high melting rates and subglacial water flow that could favour development of water drainage systems (e.g. linked cavities, meltwater channels) in-between ribbed bedforms (Perol et al., 2015; Perol and Rice, 2015).

Finally, hummocky bedforms, which have hitherto been considered exclusively as marginal landforms associated to ice stagnation and retreat (e.g. Johnson and Clayton, 2003), seem to exhibit a spatial association and a genetic proximity with the ribbed bedforms below the experimental shear margins. Some studies suggest that a morphological continuum between quasi-circular bedforms (i.e. hummocky shape) and ribbed bedforms exists below ice streams and ice sheets (Stokes et al., 2013a; Ely et al., 2016). It is thus appropriate to hypothesize a common origin for some hummocky bedforms coexisting with fields of ribbed bedforms (**Fig. 14**). They could therefore be alternately interpreted as proto-

ribbed bedforms in a continuum of subglacial bedforms inferred from the evolution of the basal shear stress intensity. The experimental results provide an array of bedforms and contexts that can be used as analogs for ice stream landsystems. However, some key bedforms observed beneath natural ice streams are not reproduced in the experiment. The absence of drumlins, MSGLs and shear moraines can be explained by several parameters inherent to the analog material we selected

620 for the modelling of ice stream-bed interactions. The low viscosity of the silicon putty and its potential high rates of creep closure prevent the formation of water-free cavities, crevasses, Nye-channels and the downstream propagation of basal ice roughness that have sometimes been proposed as prerequisites for the formation of drumlins, MSGLs and shear moraines (Bluemle et al., 1993; Punkari, 1997; Tulaczyk et al., 2001; Clark et al., 2003; Smith et al., 2007). The formation of MSGLs and drumlins has also been linked to bed roughness and lateral transitions in bed rheology and erodibility that

625 cannot be modelled considering the homogeneous, soft and even bed we intentionally use to ensure experimental reproducibility. If groove distributions and elongations reproduced in the experiments are easily comparable to MSGLs along ice stream beds, the process of formation is somehow different since MSGLs are believed to result from the ploughing and carving of ice keels into soft substratum (Clark et al., 2003) while grooves are formed by ploughing and carving of larger-size particles into the soft bed (Smith, 1948). Groove ploughing, initiated by the subglacial displacement

630 of bedrock mega rafts across a softer bed, has however been proposed to explain the formation of parallel lineations beneath palaeo-ice streams in Alberta (Atkinson et al., 2018; Evans et al., 2020).

5.3. Ribbed bedforms in ice stream landsystems

5.3.1. Implications for reconstructing the spatial organisation of ice streams

Ribbed bedforms are ubiquitous and conspicuous features covering extensive areas of former ice sheet beds (Aylsworth
635 & Shilts, 1989; Hättestrand & Kleman, 1999; Souček et al., 2015; Stokes, 2018). Their occurence along palaeo-ice stream beds and their relation with the dynamics of fast-flowing ice corridors have however been little discussed since their formation has mostly been attributed to slow ice flow. Ribbed bedforms mostly appear as isolated patches in trunks or in the onset zone of ice streams (Dyke et al., 1992; Stokes et al., 2008) and more rarely as corridors (e.g. ribbons track; Dunlop & Clark, 2006b) or belts (Greenwood & Kleman, 2010; Stokes et al., 2016) like the ones we mapped on DEMs
640 and remotely-sensed images or identified in the experiments. The coexistence of ribbed bedform patches and streamlined bedforms below ice streams has already been observed but interpreted as indicating very localized velocity gradients resulting from scattered sticky-spots (Shaw, 1979; Bouchard, 1989; Lindén et al., 2008; Stokes et al., 2008, 2016; Trommelen et al., 2014). Combining experimental and natural observations, we conclude that ribbed bedforms can constitute additional morphological markers contributing to the identification of shear margins and lobe margins (of
645 terrestrial-terminating ice streams), representing areas with high gradients of ice velocity (**Fig. 14**).

These results have new implications for the identification of palaeo-ice streams. An important point, if our conclusions hold, is that parallel ridge sequences mirroring the shape of lobate margins might often be subglacially- produced ribbed bedforms rather than proglacial thrust tectonic ridges, placing the ice margin in a different location in an ensuing reconstruction. Topographic borders and shear moraines are usually used to define the position of palaeo-shear margins.
650 Corridors of oblique and regular-spaced ribbed bedforms could be used as an additional proxy for the reconstruction of shear margin positions, notably when shear moraines are not observed or when ice streams are not controlled by the topography. In addition, multiple activations, migrations or retreats of ice streams imply the superimposition of several generations of bedforms that makes ice stream beds a complex palimpsest to decipher (e.g. Clark, 1999). Indeed, the belts of marginal bedforms mimicking the morphology of palaeo-ice lobes and swarms of streamlined bedforms characterizing
655 the position of palaeo-trunks are commonly modified through bed erosion, deformation and overprinting, thus altering

partially to fully the initial landsystems. In the light of our results, the interpretation of some fields of ribbed bedform forming successive corridors (parallel to ice flow) or belts (perpendicular to ice flow) deserves reconsideration. Depending on the orientation of the ribbed bedform long axes relative to the direction of streamlined bedforms, as well as the elongation ratio and the spacing between individual bedforms, the corridors and belts of ribbed bedforms could

660 indicate lateral and/or frontal migrations of palaeo-ice stream positions through time. Thus, this study provides additional mapping criteria to constrain the temporal migration of previously-identified palaeo-ice streams (e.g. CAIS; **Figs. 12e, f**) and potentially identify new ones through the identification of their margins, particularly when features such as MSGL are poorly-preserved or absent.

5.3.2. Implications for ice stream dynamics and subglacial hydrology

665 The combination of analog modelling and ice stream bed mapping has allowed us to establish a link between bedform development, ice stream dynamics and the evolution of spatially and temporally efficient drainage systems (**Fig. 14**). The efficiency of the subglacial drainage system is estimated by the capacity of channelized features (e.g. tunnel valleys and meltwater channels) to accommodate the meltwater discharge (Moon et al., 2014). Thus, considering the relationships between the distribution of subglacial water, the development of channelized features and the development of ribbed

670 bedforms below experimental lobes, we suggest that the presence or absence of submarginal ribbed bedforms along lobate margins might reveal the type and efficiency of meltwater drainage below marginal lobes of terrestrially-terminating ice streams (Raymond, 1987; Patterson, 1997; Kim et al., 2016). For instance, well-developed channelization facilitates subglacial drainage by focusing meltwater flow into tunnel valleys and induces an overall increase of basal drag beneath the lobe due to water pressure reduction, widespread ice-bed coupling and elevated basal shear stress. The increase in

675 basal drag, highlighted by the development of submarginal ribbed bedforms, is responsible for ice stream slowdown and stabilization of the marginal lobe. This configuration should be associated with the development of well-developed end moraines (**Fig. 14**), because the margin experiences a stillstand over time. Conversely, a poorly-developed channelization characterized by shallow and narrow meltwater channels reveals the incapacity of the subglacial drainage system to evacuate all the meltwater efficiently. This configuration is more likely characterized by higher water pressure,

680 widespread ice-bed decoupling and distributed drainage that promote basal sliding and inhibits the formation of ribbed bedforms in sub-marginal environments. The inefficient drainage might favour the storage of meltwater up-ice during periods of increased melting that is episodically delivered to the margin through outburst floods. We suggest that outburst flood events and basal sliding could alter the dynamics of ice streams and trigger surging of ice lobes. The absence of submarginal ribbed bedforms and a poorly-developed drainage system should therefore be associated with typical surge-

685 diagnostic features dominated by compressional structures (**Fig. 14**). Glaciotectonic thrust masses and crevasse-squeezed ridges have notably been observed in southeast Alberta and linked to the dynamics of surging lobes during melting and retreat of the Laurentide Ice Sheet (Evans et al., 2020).

6. Conclusion

Despite the ubiquitous and extensive nature of subglacially-produced ribbed landforms beneath former ice sheets

690 (variously called Rogen moraine, ribbed moraine, ribbed bedforms, traction ribs, mega-scale transverse ridges), their significance in ice stream landsystems and their formation processes remain poorly understood. Providing new constraints on the formation, evolution and distribution of ribbed bedforms is therefore critical to characterize ice-bed interactions beneath key zones of ice streams and reconstruct past glacial dynamics. Based on experimental modelling and geomorphological mapping of natural ice stream beds, we suggest that a type of subglacial ribs, that we call ribbed

The Cryosphere
Discussions

695 bedforms, are produced subglacially beneath ice streams margins where the soft bed is coupled to the ice and subject to high basal shear stresses that results from abrupt spatial variations in subglacial drainage characteristics and ice flow velocity. We suggest that these ribbed bedforms develop both (i) in narrow corridors parallel to lineations and (ii) in broad belts parallel to and upstream of marginal landforms. The first ones (i.e., lateral ribbed bedforms) can be used to highlight the position of ice stream shear margins. These ribbed bedforms are regularly-spaced, slightly arcuate and moderately

700 elongated (l/w = 3 to 4). In our experiments high shear strain rates along shear margins lead to the rotation of the long-axis of ribs setting them oblique to the palaeo-ice flow direction. This oblique relationship has implications for those reconstructing palaeo ice flow directions (flow sets) from bedforms, where misinterpretation could be made using the usual assumption of ribs forming orthogonal to flow. The second ones (i.e., submarginal ribbed bedforms) form larger belts of coalescent and broad ribbed bedforms characterized by arcuate crests arranged orthogonal to the ice flow

705 direction. They are interpreted as the morphological imprints of ice lobe positions, but unlike the usual belt of marginal landforms hitherto described in the literature and interpreted as proglacial glaciotectonic structures this type of ribbed bedforms initiates and develops subglacially from the basal shearing of a flat subglacial bed. Their preferential development in interfluve areas between meltwater channels implies that their formation is enhanced in zones of channelized and efficient drainage where extensive areas of ice-bed coupling exists due to the decrease of subglacial

710 water pressure. We therefore suggest that those two specific kinds of ribbed bedforms (i.e. lateral and submarginal) result from an identical process in the underlying soft bed that accommodate high basal shear stress either through plastic deformation or sediment flow and accretion.

These results provide new criteria for palaeo-glaciological reconstructions of ice streams helping identify shear and lobe margins and provide insights on ice-bed interactions, ice dynamics and subglacial hydrology. Whether the process of

715 ribbed bedforms discussed here in the context of ice streams and lobes is relevant and applicable more widely to the full population of ribbed / Rogen moraines found extensively across many ice sheet beds, is still an open question.

730

The Cryosphere
Discussions

Open Access

EGU

References

Aario, R.: Classification and terminology of morainic landforms in Finland. Boreas, 6(2), 87–100, https://doi.org/10.1111/j.1502-3885.1977.tb00338.x, 1977.

Alley, R. B.: In search of ice-stream sticky spots. Journal of Glaciology, 39(133), 447–454, https://doi.org/10.3189/s0022143000016336, 1993.

735 Atkinson, N., Utting, D. J., and Pawley, S. M.: An Update to the Glacial Landforms Map of Alberta. In Alberta Geological Survey, https://doi.org/10.13140/RG.2.2.20500.40320, 2018.

Atkinson, N., Pawley, S., and Utting, D. J.: Flow-pattern evolution of the Laurentide and Cordilleran ice sheets across west-central Alberta, Canada: implications for ice sheet growth, retreat and dynamics during the last glacial cycle. Journal of Quaternary Science, 31(7), 753–768, https://doi.org/10.1002/jqs.2901, 2016.

740 Aylsworth, J. M., and Shilts, W. W.: Bedforms of the Keewatin Ice Sheet, Canada. Sedimentary Geology, 62(2–4), 407–428, https://doi.org/10.1016/0037-0738(89)90129-2, 1989.

Bamber, J. L., Vaughan, D. G., and Joughin, I.: Widespread complex flow in the interior of the antarctic ice sheet. Science, 287(5456), 1248–1250, https://doi.org/10.1126/science.287.5456.1248, 2000.

Barchyn, T. E., Dowling, T. P. F., Stokes, C. R., and Hugenholtz, C. H.: Subglacial bed form morphology controlled by ice speed and sediment thickness.

745 Geophysical Research Letters, 43(14), 7572–7580, https://doi.org/10.1002/2016GL069558, 2016.

Benn, D. I., & Evans, D. J. A.: Glaciers and glaciation, 2nd Edition, Hodder Arnold Publication, 2010.

Benn, D.I.: The genesis and significance of hummocky moraine: evidence frome the isle of Skye, Scotland. Quaternary Research (United States), 11, 781–799, https://doi.org/10.1016/0277-3791(92)90083-K, 1992.

Bluemle, J. P., Lord, M. L., and Hunke, N. T.: Exceptionnaly long, narrow drumlins formed in subglacial cavities, North Dakota. Boreas, 22, 15–24,

750 https://doi.org/10.4135/9781544354453.n41, 1993.

Boone, S. J., and Eyles, N.: Geotechnical model for great plains hummocky moraine formed by till deformation below stagnant ice, Geomorphology, 38(1–2), 109–124, https://doi.org/10.1016/S0169-555X(00)00072-6, 2001.

Bouchard, M. A.: Subglacial landforms and deposits in central and northern Québec, Canada, with emphasis on Rogen moraines. Sedimentary Geology, 62(2–4), 293–308, https://doi.org/10.1016/0037-0738(89)90120-6, 1989.

755 Bougamont, M., Price, S. F., Christoffersen, P., and Payne, A. J.: Dynamic patterns of ice stream flow in a 3-D higher-order ice sheetmodel with plastic bed and simplified hydrology. Journal of Geophysical Research, 116, 1–13, https://doi.org/10.1029/2011JF002025, 2011.

Boulton, G. S.: Push-moraines and glacier-contact fans in marine and terrestrial environments. Sedimentology, 33(5), 677–698, https://doi.org/10.1111/j.1365-3091.1986.tb01969.x, 1986.

Boulton, G. S.: A theory of drumlin formation by subglacial sediment deformation. In Drumlin symposium. Manchester, 1985 (pp. 25–80), 1987.

760 Boulton, G. S., and Hindmarsh, R. C. A.: Sediment deformation beneath glaciers: rheology and geological consequences. Journal of Geophysical Research, 92(B9), 9059–9082, https://doi.org/10.1029/JB092iB09p09059, 1987.

Boyce, J. I., and Eyles, N.: Drumlins carved by deforming till streams below the Laurentide Ice Sheet. Geology, 19(8), 787–790, https://doi.org/10.1130/0091-7613(1991)019<0787:DCBDTS>2.3.CO;2, 1991.

Briner, J. P.: Supporting evidence from the New York drumlin field that elongate subglacial bedforms indicate fast ice flow. Boreas, 36(2), 143–147,

765 https://doi.org/10.1080/03009480600923394, 2007.

Chandler, B. M. P., Evans, D. J. A., and Roberts, D. H.: Characteristics of recessional moraines at a temperate glacier in SE Iceland: Insights into patterns, rates and drivers of glacier retreat. Quaternary Science Reviews, 135, 171–205, https://doi.org/10.1016/j.quascirev.2016.01.025, 2016.

Chapwanya, M., Clark, C. D., and Fowler, A. C.: Numerical computations of a theoretical model of ribbed moraine formation. Earth Surface Processes and Landforms, 36(8), 1105–1112. https://doi.org/10.1002/esp.2138, 2011.

770 Clark, C. D.: Glaciodynamic context of subglacial bedform generation and preservation. Annals of Glaciology, 28, 23–32. https://doi.org/10.3189/172756499781821832, 1999.

Clark, C. D., and Stokes, C. R.: Palaeo-ice stream landsystem. In Glacial Landsystems, pp. 204–227, 2003.

Clark, C. D.: Emergent drumlins and their clones: from till dilatancy to flow instabilities. Journal of Glaciology, 56(200), 1011-1025, https://doi.org/10.3189/002214311796406068, 2010.

775 Clark, C. D., Ely, J. C., Spagnolo, M., Hahn, U., Hughes, A. L., and Stokes, C. R.: Spatial organization of drumlins. Earth Surface Processes and Landforms, 43(2), 499-513, https://doi.org/10.1002/esp.4192, 2018.

Clark, C. D., Tulaczyk, S. M., Stokes, C. R., and Canals, M.: A groove-ploughing theory for the production of mega-scale glacial lineations, and implications for ice-stream mechanics. Journal of Glaciology, 49(165), 240–256, https://doi.org/10.3189/172756503781830719, 2003.

Cofaigh, C. Ó.: Tunnel valley genesis. Progress in Physical Geography: Earth and Environment, 20(1), 1–19,

780 https://doi.org/10.1177/030913339602000101, 1996.

Cowan, W. R.: Ribbed moraine: Till-fabric analysis and origin. Canadian Journal of Earth Sciences, 5(5), 1145–1159, https://doi.org/10.1139/e68-112, 1968.

De Angelis, H., and Kleman, J.: Palaeo-ice streams in the Foxe/Baffin sector of the Laurentide Ice Sheet. Quaternary Science Reviews, 26(9–10), 1313–1331, https://doi.org/10.1016/j.quascirev.2007.02.010, 2007.

785 Denton, G. H., and Hughes, T.: The last great ice sheets. https://doi.org/10.1111/1467-8489.00221, 1981.

Dunlop, P., and Clark, C. D.: The morphological characteristics of ribbed moraine. Quaternary Science Reviews, 25(13–14), 1668–1691, https://doi.org/10.1016/j.quascirev.2006.01.002, 2006.

Dunse, T., Schellenberger, T., Hagen, J. O., Kääb, A., Schuler, T. V., and Reijmer, C. H.: Glacier-surge mechanisms promoted by a hydro-thermodynamic feedback to summer melt. Cryosphere, 9(1), 197–215, https://doi.org/10.5194/tc-9-197-2015, 2015.

790 Dyke, A. S., Morris, T. F., Green, D. E. C., and England, J.: Quaternary geology of Prince of Wales Island, Arctic Canada. In Memoir - Geological Survey of Canada (Vol. 433), https://doi.org/10.4095/134058, 1992.

Dyke, A. S., and Morris, T. F.: Drumlin fields, dispersal trains and ice streams in Arctic Canada. Canadian Geographer / Le Géographe Canadien, 32(1), 86–90, https://doi.org/10.1111/j.1541-0064.1988.tb00860.x, 1988.

Ebert, K., and Kleman, J.: Circular moraine features on the Varanger Peninsula, northern Norway, and their possible relation to polythermal ice sheet
795 coverage. Geomorphology, 62(3–4), 159–168, https://doi.org/10.1016/j.geomorph.2004.02.009, 2004.

Echelmeyer, K. A., Harrison, W. D., Larsen, C., and Mitchell, J. E.: The role of the margins in the dynamics of an active ice stream. Journal of Glaciology, 40(136), 527–538, https://doi.org/10.3189/S0022143000012417, 1994.

Ely, J. C., Clark, C. D., Spagnolo, M., Stokes, C. R., Greenwood, S. L., Hughes, A. L. C., Dunlop, P., and Hess, D.: Do subglacial bedforms comprise a size and shape continuum? Geomorphology, 257, 108–119, https://doi.org/10.1016/j.geomorph.2016.01.001, 2016.

800 Engelhardt, H., Humphrey, N., Kamb, B., and Fahnestock, M.: Physical conditions at the base of a fast moving Antarctic ice stream. Science, 248(4951), 57–59, https://doi.org/10.1126/science.248.4951.57, 1990.

Evans, D. J. A., Atkinson, N., and Phillips, E.: Glacial geomorphology of the Neutral Hills Uplands, southeast Alberta, Canada: The process-form imprints of dynamic ice streams and surging ice lobes. Geomorphology, 350, 106910, https://doi.org/10.1016/j.geomorph.2019.106910, 2020.

Evans, D. J. A., Clark, C. D., and Rea, B. R.: Landform and sediment imprints of fast glacier flow in the southwest Laurentide Ice Sheet. Journal of
805 Quaternary Science, 23(3), 249–272, https://doi.org/10.1002/jqs, 2008.

Evans, D. J. A., and Hiemstra, J. F.: Till deposition by glacier submarginal, incremental thickening. Earth Surface Processes and Landforms, 30(13), 1633–1662, https://doi.org/10.1002/esp.1224, 2005.

Evans, D. J. A., Young, N. J. P., and Cofaigh, C. O.: Glacial geomorphology of terrestrial-terminating fast flow lobes/ice stream margins in the southwest Laurentide Ice Sheet. Geomorphology, 204, 86–113, https://doi.org/10.1016/j.geomorph.2013.07.031, 2014.

810 Evans, D.J.A., Ewertowski, M., Orton, C.:. Fláajökull (north lobe), Iceland: active temperate piedmont lobe glacial landsystem. Journal of Maps, http://dx.doi.org/10.1080/17445647.2015.1073185, 2015.

Evans, D. J., Storrar, R. D., & Rea, B. R.: Crevasse-squeeze ridge corridors: diagnostic features of late-stage palaeo-ice stream activity. Geomorphology, 258, 40-50, https://doi.org/10.1016/j.geomorph.2016.01.017, 2016.

Eyles, N., Boyce, J. I., and Barendregt, R. W.: Hummocky moraine: Sedimentary record of stagnant Laurentide Ice Sheet lobes resting on soft beds.
815 Sedimentary Geology, 123(3–4), 163–174, https://doi.org/10.1016/S0037-0738(98)00129-8, 1999.

Fannon, J. S., Fowler, A. C., and Moyles, I. R.: Numerical simulations of drumlin formation. Proceedings of the Royal Society A: Mathematical, Physical and Engineering Sciences, 473(2204), https://doi.org/10.1098/rspa.2017.0220, 2017.

Fowler, A. C.: An instability mechanism for drumlin formation. Geological Society Special Publication, 176(1987), 307–319, https://doi.org/10.1144/GSL.SP.2000.176.01.23, 2000.

820 Fowler, A. C., and Chapwanya, M.: An instability theory for the formation of ribbed moraine, drumlins and mega-scale glacial lineations. Proceedings of the Royal Society A: Mathematical, Physical and Engineering Sciences, 470(2171), https://doi.org/10.1098/rspa.2014.0185, 2014.

Goldstein, R., Engelhardt, H. F., Kamb, B., and Frolich, R.: Satellite Radar lnterferometry for Monitoring lce-sheet Motion: application to Antarctic Ice Stream. Science, 262(5139), 1525–1530, https://doi.org/10.1126/science.262.5139.1525, 1993.

Greenwood, S. L., and Clark, C. D.: Subglacial bedforms of the Irish ice sheet. Journal of Maps, 4(1), 332-357, https://doi.org/10.4113/jom.2008.1030,
825 2008.

Greenwood, S. L., and Kleman, J.: Glacial landforms of extreme size in the Keewatin sector of the Laurentide Ice Sheet. Quaternary Science Reviews, 29(15–16), 1894–1910, https://doi.org/10.1016/j.quascirev.2010.04.010, 2010.

Hättestrand, C., and Kleman, J.: Ribbed moraine formation. Quaternary Science Reviews, 18(1), 43–61, https://doi.org/10.1016/S0277-3791(97)00094-2, 1999.

830 Hindmarsh, R. C. A.: Drumlinization and drumlin-forming instabilities: Viscous till mechanisms. Journal of Glaciology, 44(147), 293–314, https://doi.org/10.1017/S002214300000263X, 1998.

Hooke, R. L., and Jennings, C. E.: On the formation of the tunnel valleys of the southern Laurentide ice sheet. Quaternary Science Reviews, 25(11-12), 1364-1372, https://doi.org/10.1016/j.quascirev.2006.01.018, 2006.

Hughes, O.: Surficial geology, Nichicun-Kaniapiskau map-area, Quebec, 1964.

835 Johnson, M. D., and Clayton, L.: Supraglacial landsystems in lowland terrain. In Glacial Landsystems, pp. 228–258, 2003.

Kim, B.-H., Lee, C.-K., Seo, K.-W., Lee, W. S., and Scambos, T.: Active subglaical lakes beneath the stagnant trunk of Kamb Ice Stream: evidence of channelized subglacial flow. The Cryosphere Discussions, April, 1–15, https://doi.org/10.5194/tc-2016-9, 2016.

Kjær, K. H., and Krüger, J.: The final phase of dead-ice moraine development: processes and sediment architecture, Kötlujökull , Iceland. Sedimentology, 48, 935–952, https://doi.org/10.1046/j.1365-3091.2001.00402.x, 2001.

840 Kleman, J., and Borgström, I.: Reconstruction of palaeo-ice sheets: The use of geomorphological data. Earth Surface Processes and Landforms, 21(10), 893–909, https://doi.org/10.1002/(SICI)1096-9837(199610)21:10<893::AID-ESP620>3.0.CO;2-U, 1996.

Lelandais, T., Mourgues, R., Ravier, É., Pochat, S., Strzerzynski, P., and Bourgeois, O.: Experimental modeling of pressurized subglacial water flow: Implications for tunnel valley formation. Journal of Geophysical Research: Earth Surface, 121(11), 2022–2041, https://doi.org/10.1002/2016JF003957, 2016.

845 Lelandais, T., Ravier, É., Pochat, S., Bourgeois, O., Clark, C., Mourgues, R., and Strzerzynski, P.: Modelled subglacial floods and tunnel valleys control the life cycle of transitory ice streams. Cryosphere, 12(8), 2759–2772, https://doi.org/10.5194/tc-12-2759-2018, 2018.

Lindén, M., Möller, P., and Adrielsson, L.: Ribbed moraine formed by subglacial folding, thrust stacking and lee-side cavity infill. Boreas, 37(1), 102–131, https://doi.org/10.1111/j.1502-3885.2007.00002.x, 2008.

Lundqvist, J.: Problems of the so-called Ribbed moraines, 1969.

850 Lundqvist, J.: Rogen (ribbed) moraine-identification and possible origin. Sedimentary Geology, 62(2–4), 281–292, https://doi.org/10.1016/0037-0738(89)90119-X, 1989.

Margold, M., Stokes, C. R., and Clark, C. D.: Ice streams in the Laurentide Ice Sheet: Identification, characteristics and comparison to modern ice sheets. Earth-Science Reviews, 143, 117–146, https://doi.org/10.1016/j.earscirev.2015.01.011, 2015.

Margold, M., Stokes, C. R., and Clark, C. D.: Reconciling records of ice streaming and ice margin retreat to produce a palaeogeographic reconstruction
855 of the deglaciation of the Laurentide Ice Sheet. Quaternary Science Reviews, 189, 1–30, https://doi.org/10.1016/j.quascirev.2018.03.013, 2018.

Marich, A., Batterson, M., and Bell, T.: The Morphology and Sedimentological Analyses of Rogen Moraines, Central Avalon Peninsula, Newfoundland. Current Research, 1–14, 2005.

Menzies, J.: A review of the literature on the formation and location of drumlins. Earth Science Reviews, 14(4), 315–359, https://doi.org/10.1016/0012-8252(79)90093-X, 1979.

860 Möller, P.: Rogen moraine: An example of glacial reshaping of pre-existing landforms. Quaternary Science Reviews, 25(3–4), 362–389, https://doi.org/10.1016/j.quascirev.2005.01.011, 2006.

Möller, P.: Melt-out till and ribbed moraine formation, a case study from south Sweden. Sedimentary Geology, 232(3–4), 161–180, https://doi.org/10.1016/j.sedgeo.2009.11.003, 2010.

Moon, T., Joughin, I., Smith, B., Van Den Broeke, M. R., Van De Berg, W. J., Noël, B., and Usher, M.: Distinct patterns of seasonal Greenland glacier
865 velocity. Geophysical Research Letters, 41(20), 7209–7216, https://doi.org/10.1002/2014GL061836, 2014.

Newton, M., Evans, D. J. A., Roberts, D. H., and Stokes, C. R.: Bedrock mega-grooves in glaciated terrain: A review. Earth-Science Reviews, 185(March 2017), 57–79, https://doi.org/10.1016/j.earscirev.2018.03.007, 2018.

Nye, J. F.: The motion of ice sheets and glaciers. Journal of Glaciology, 3(26), 493–507, https://doi.org/10.3189/s002214300001724x, 1959.

Paterson, W. S. B.: The Physics of Glaciers, 3rd Edition, Pergamon, 1994.

870 Patterson, C. J.: Southern Laurentide ice lobes were created by ice streams: Des Moines Lobe in Minnesota, USA. Sedimentary Geology, 111(1–4), 249–261, https://doi.org/10.1016/S0037-0738(97)00018-3, 1997.

Perol, T., and Rice, J. R.: Shear heating and weakening of the margins of West Antarctic ice streams. May, 3406–3413, https://doi.org/10.1002/2015GL063638, 2015.

Perol, T., Rice, J. R., Platt, J. D., and Suckale, J.: Subglacial hydrology and ice stream margin locations Special Section : Journal of Geophysical
875 Research: Earth Surface, 1352–1368, https://doi.org/10.1002/2015JF003542, 2015.

Porter, C., Morin, P., Howat, I., Noh, M.-J., Bates, B., Peterman, K., Keesey, S., Schlenk, M., Gardiner, J., Tomko, K., Willis, M., et al., ArcticDEM. Harvard Dataverse, V1. 2018.

Punkari, M.: Glacial and glaciofluvial deposits in the interlobate areas of the Scandinavian Ice Sheet. Quaternary Science Reviews, 16(97), 741–753, https://doi.org/10.1016/S0277-3791(97)00020-6, 1997.

880 Ramsay, J., and Huber, M.: The techniques of modern structural geology: Folds and fractures, Elsevier Science, 1987.

Raymond, C. F.: How Do Glaciers Surge? A Review. Journal of Geophysical Research, 92(B9), 9121–9134, https://doi.org/10.1029/JB092iB09p09121,1987.

Raymond, C. F., Echelmeyer, K. A., Whillans, I. M., and Doake, C. S. M. (2001). Ice stream shear margins. Antarctic Research Series, 77, 137–155, https://doi.org/10.1029/AR077p0137, 2001.

885 Rose, J.: Drumlins as part of a glacier bedform continuum. In Drumlin symposium. Balkema, Rotterdam, https://doi.org/10.1111/jawr.2010.46.issue-5, 1987.

Sarala, P.: Ribbed moraine stratigraphy and formation in southern Finnish Lapland. Journal of Quaternary Science, 21(4), 387–398, https://doi.org/10.1002/jqs.995, 2006.

Schellenberger, T., Dunse, T., Kääb, A., Schuler, T. V., Hagen, J. O., and Reijmer, C. H.: Multi-year surface velocities and sea-level rise contribution
890 of the Basin-3 and Basin-2 surges, Austfonna, Svalbard. The Cryosphere Discussions, February, 1–27, https://doi.org/10.5194/tc-2017-5, 2017.

Schoof, C.: Pressure-dependent viscosity and interfacial instability in coupled ice-sediment flow. Journal of Fluid Mechanics, 570(February), 227–252, https://doi.org/10.1017/S0022112006002874, 2007.

Sergienko, O. V., Creyts, T. T., and Hindmarsh, R. C. A.: Similarity of organized patterns in driving and basal stresses of Antarctic and Greenland ice sheets beneath extensive areas of basal sliding. Geophysical Research Letters, 41(11), 3925–3932, https://doi.org/10.1002/2014GL059976, 2014.

895 Sergienko, O. V., and Hindmarsh, R. C. A.: Regular patterns in frictional resistance of ice-stream beds seen by surface data inversion. Science, 342(November), 1086–1089, https://doi.org/10.1126/science.1243903, 2013.

Sevestre, H., Benn, D. I., Luckman, A., Nuth, C., Kohler, J., Lindbäck, K., and Pettersson, R. (2018). Tidewater Glacier Surges Initiated at the Terminus. Journal of Geophysical Research: Earth Surface, 123(5), 1035–1051, https://doi.org/10.1029/2017JF004358, 2018.

Sharp, M.J.: "Crevasse-fill" ridges — a landform type characteristic of surging? Geogr. Ann. A67, 213–220,
900 https://doi.org/10.1080/04353676.1985.11880147, 1985.

Shaw, J. (1979). Genesis of the Sveg tills and Rogen moraines of central Sweden: a model of basal melt out. Boreas, 8(4), 409–426, https://doi.org/10.1111/j.1502-3885.1979.tb00437.x, 1979.

Smith, A. M., Murray, T., Nicholls, K. W., Makinson, K., Adalgeirsdóttir, G., Behar, A. E., and Vaughan, D. G.: Rapid erosion, drumlin formation, and changing hydrology beneath an Antarctic ice stream. Geology, 35(2), 127–130, https://doi.org/10.1130/G23036A.1, 2007.

905 Smith, H. T. U.: Giant glacial grooves in northwest Canada. American Journal of Science, 246(8), 503–514, https://doi.org/10.2475/ajs.246.8.503, 1948.

Souček, O., Bourgeois, O., Pochat, S., and Guidat, T.: A 3 Ga old polythermal ice sheet in Isidis Planitia, Mars: Dynamics and thermal regime inferred from numerical modeling. Earth and Planetary Science Letters, 426, 176–190, https://doi.org/10.1016/j.epsl.2015.06.038, 2015.

Stokes, C. R.: Geomorphology under ice streams: Moving from form to process. Earth Surface Processes and Landforms, 43(1), 85–123, https://doi.org/10.1002/esp.4259, 2018.

910 Stokes, C. R, and Clark, C. D.: Palaeo-ice streams. Quaternary Science Reviews, 20, 1437–1457, https://doi.org/10.1016/S0277-3791(01)00003-8, 2001.

Stokes, C. R., and Clark, C. D.: Are long subglacial bedforms indicative of fast ice flow? Boreas, 31(3), 239–249. https://doi.org/10.1111/j.1502-3885.2002.tb01070.x, 2002a.

Stokes, C. R., and Clark, C. D.: Ice stream shear margin moraines. Earth Surface Processes and Landforms, 27(5), 547–558.
915 https://doi.org/10.1002/esp.326, 2002b.

Stokes, C.R., and Clark, C.D.: The Dubawnt Lake palaeo-ice stream: evidence for dynamic ice sheet behaviour on the Canadian Shield and insights regarding the controls on ice-stream location and vigour. Boreas, 32(1), 263–279, https://doi.org/10.1080/03009480310001155, 2003.

Stokes, C. R., Clark, C. D., Lian, O. B., and Tulaczyk, S.: Geomorphological map of ribbed moraines on the Dubawnt Lake Palaeo-Ice Stream bed: A signature of ice stream shut-down? Journal of Maps, 2(1), 1–9, https://doi.org/10.4113/jom.2006.43, 2006a.

920 Stokes, C. R., Clark, C. D., and Winsborrow, C. M.: Subglacial bedform evidence for a major palaeo-ice stream and its retreat phases in Amundsen Gulf, Canadian Arctic Archipelago. Journal of Quaternary Science, 21(4), 399–412, https://doi.org/10.1002/jqs.991, 2006b.

Stokes, C. R., Clark, C. D., Lian, O. B., and Tulaczyk, S.: Ice stream sticky spots: A review of their identification and influence beneath contemporary and palaeo-ice streams. Earth-Science Reviews, 81(3–4), 217–249, https://doi.org/10.1016/j.earscirev.2007.01.002, 2007.

Stokes, C. R., Lian, O. B., Tulaczyk, S., and Clark, C. D.: Superimposition of ribbed moraines on a palaeo-ice-stream bed: implications for ice stream
925 dynamics and shutdown. Earth Surface Processes and Landforms, 33, 593–609, https://doi.org/10.1002/esp, 2008.

Stokes, C. R., Spagnolo, M., Clark, C. D., Ó Cofaigh, C., Lian, O. B., and Dunstone, R. B.: Formation of mega-scale glacial lineations on the Dubawnt Lake Ice Stream bed: 1. size, shape and spacing from a large remote sensing dataset. Quaternary Science Reviews, 77, 190–209, https://doi.org/10.1016/j.quascirev.2013.06.003, 2013a.

Stokes, C. R., Fowler, A. C., Clark, C. D., Hindmarsh, R. C., and Spagnolo, M.: The instability theory of drumlin formation and its explanation of their
930 varied composition and internal structure. Quaternary Science Reviews, 62, 77-96, https://doi.org/10.1016/j.quascirev.2012.11.011, 2013b.

Stokes, C. R., Margold, M., and Creyts, T. T.: Ribbed bedforms on palaeo-ice stream beds resemble regular patterns of basal shear stress ('traction ribs') inferred from modern ice streams. Journal of Glaciology, 62(234), 696–713, https://doi.org/10.1017/jog.2016.63, 2016.

Totten, S. M.: Overridden Recessional Moraines of North-Central Ohio. GSA Bulletin ; 80 (10): 1931–1946, https://doi.org/10.1130/0016-7606(1969)80[1931:ORMONO]2.0.CO;2, 1969.

935 Trommelen, M. S., Ross, M., and Ismail, A.: Ribbed moraines in northern Manitoba, Canada: Characteristics and preservation as part of a subglacial bed mosaic near the core regions of ice sheets. Quaternary Science Reviews, 87, 135–155. https://doi.org/10.1016/j.quascirev.2014.01.010, 2014.

Tulaczyk, S. M., Kamb, W. B., and Engelhardt, H. F.: Basal mechanics of Ice Stream B, West Antarctica 2. Undrained plastic bed model. Journal of Geophysical Research, 105(B1), 483–494, https://doi.org/10.1029/1999JB900328, 2000.

Tulaczyk, Slawek M., Scherer, R. P., and Clark, C. D.: A ploughing model for the origin of weak tills beneath ice streams: A qualitative treatment.

940   Quaternary International, 86(1), 59–70. https://doi.org/10.1016/S1040-6182(01)00050-7, 2001.

Winsborrow, M. C. M., Clark, C. D., and Stokes, C. R.: Ice streams of the Laurentide Ice Sheet. Geographie Physique et Quaternaire, 58(2–3), 269–280. https://doi.org/10.7202/013142ar, 2004.

Zheng, W., Pritchard, M. E., Willis, M. J., and Stearns, L. A.: The Possible Transition From Glacial Surge to Ice Stream on Vavilov Ice Cap. Geophysical Research Letters, 46(23), 13892–13902. https://doi.org/10.1029/2019GL084948, 2019.

945